

## **Magnetic Mineralogical Approach for Exploration of Gas Hydrates in the Bay of Bengal**

**Firoz Badesab<sup>1</sup>, Pawan Dewangan<sup>1</sup>, Virsen Gaikwad<sup>1</sup>, Myriam Kars<sup>2</sup>, Muralidhar Kocherla<sup>1</sup>, Kolluru S. Krishna<sup>3</sup>, Satish J. Sangode<sup>4</sup>, Kannan Deenadayalan<sup>5</sup>, Pushendra Kumar<sup>6</sup>, Omkar Naikgaonkar<sup>1</sup>, Mohammad Ismaiel<sup>3</sup>, and Aarbaz Khan<sup>1</sup>**

<sup>1</sup> CSIR - National Institute of Oceanography, Dona Paula 403004, Goa, India

<sup>2</sup> Centre for Advanced Marine Core Research, Kochi University, Nankoku, Japan

<sup>3</sup> Centre for Earth and Space Sciences, University of Hyderabad, India

<sup>4</sup> Department of Geology, Savitribai Phule Pune University, Pune-411007, India

<sup>5</sup> Indian Institute of Geomagnetism, New Panvel, Navi Mumbai, India

<sup>6</sup> Oil and Natural Gas Corporation Ltd., Institute of Engineering and Ocean Technology, Panvel, Navi Mumbai, India

Corresponding author: Firoz Badesab (firoz@nio.org)

### **Abstract**

We evaluate environmental magnetic, geochemical, and sedimentological records from three sediment cores from potential methane-hydrate bearing sites to unravel linkages between sedimentation, shale-tectonics, magnetite enrichment, diagenesis, and gas hydrate formation in the Krishna-Godavari (K-G) basin. Based on down-core rock magnetic variations, four sedimentary magnetic property zones (I-IV) are demarcated. A uniform band of enhanced magnetic susceptibility (zone-III) appears to reflect a period of high sedimentation events in the K-G basin. Highly pressurized sedimentary strata developed as a result of increased sedimentation that triggered development of a fault system that provided conduits for upward methane migration to enter the gas hydrate stability zone (GHSZ) leading to formation of gas hydrate deposits and potentially seal the fault system. Magnetic susceptibility fluctuations and the presence of iron sulfides in a magnetically enhanced zone suggests that fault system growth facilitated episodic methane venting from deeper sources that led to multiple methane seepage events. Pyrite formation along sediment fractures resulted in diagenetic depletion of magnetic signals and potentially indicates paleo sulfate-methane transition zone positions. We demonstrate that a close correlation between magnetic susceptibility and chromium reducible sulfur concentration can be used as a proxy to constrain paleo-methane seepage events. Our findings suggest that the interplay between higher sedimentation events and shale-tectonism facilitated fluid/gas migration and trapping, and development of the gas hydrate system in the K-G basin. The proposed magnetic mineralogical approach has wider scope to constrain understanding of gas hydrate systems in marine sediments.

### **Key Points:**

- We present a rock magnetic record of high sedimentation events in Bay of Bengal.
- We investigate the controls of rapid sedimentation and shale-tectonism on development of the fracture-filled gas hydrate system in Krishna-Godavari (K-G) basin.
- We have developed a magnetic proxy to constrain paleo-CH<sub>4</sub> seepage events in marine sediments.

## 1. Introduction

Gas Hydrates are distributed widely in oceanic and permafrost regions, and store immense quantities of methane gas (Kvenvolden, 1993). In the last few decades, there has been emphasis on understanding natural gas hydrate reservoirs as potential alternative energy resources (Boswell & Collett, 2011; Kvenvolden, 1988), for estimating global carbon budgets (Dickens et al., 1995), and for understanding the role of methane as a greenhouse gas and significant contributor to climate change (Archer & Buffett, 2005; Kennett et al., 2000). Geodynamics, tectonism, global climatic change, sea level fluctuations, and variable sedimentation rate can affect development of gas hydrate systems in marine sedimentary environments (García-Tortosa et al., 2011; Herbozo et al., 2013; Moore et al., 2015; Milkov & Sassen, 2002; Paull et al., 1991). For example, neotectonic activity can potentially alter the base of the gas hydrate stability zone (GHSZ) leading to gas hydrate dissociation and intensified methane expulsion/seepage events (Dewangan et al., 2008; Goto et al., 2016; Jahren et al., 2005; Riedel et al., 2011; von Huene & Pecher, 1999). Rapid sediment loading triggered by abrupt climatic changes, and supply from major river systems can generate over-pressured sedimentary strata, thereby creating an efficient fluid migration system and sedimentary reservoir for methane trapping and gas hydrate formation (Hustoft et al., 2009; Karsten et al., 2018; Torres et al., 2008; Wang et al 2011b; Yu et al., 2014).

Magnetic iron minerals are widespread and indicative of sedimentary constituents and their associated magnetic signals can reflect primary depositional and secondary diagenetic processes (Canfield, 1989). Sediment provenance, sedimentation rate, transportation, and depositional conditions determine the concentration, grain size, and mineralogy of magnetic minerals and can significantly affect sediment magnetic records (Thompson & Oldfield, 1986; Verosub & Roberts, 1995). Diagenetic processes can also lead to primary magnetic mineral dissolution and precipitation of secondary magnetic minerals (Roberts, 2015). Soon after deposition, primary iron mineral assemblages pass through a sequence of early diagenetic processes in which the minerals undergo alteration. One major pathway is the reaction with hydrogen sulfide via sulfate reduction coupled with anaerobic oxidation of methane (AOM) which is driven by bacterial organic matter decomposition (Berner, 1970; Canfield, 1989; Ferdelman et al., 1999; Froelich et al., 1979; Jørgensen, 1982). Diagenetic reactions involved in iron (oxyhydr)oxide reduction by hydrogen sulfide and subsequent iron sulfide formation is well described by Karlin & Levi (1983) and Channell & Hawthorne (1990).

In gas hydrate environments, AOM is an important biogeochemical process that results from the interaction of upward methane flux and downward sulfate flux (Knittel & Boetius, 2009; Treude et al., 2005). Sulfate reduction coupled with AOM generates huge amounts of hydrogen sulfide into pore waters, which reacts further with dissolved iron to form magnetic iron sulfides thereby creating distinct secondary magnetic signals in the AOM zone (Berner, 1970; Canfield & Berner, 1987; Dewangan et al., 2013; Jørgensen et al., 2004; Leslie et al., 1990; Riedinger et al., 2005, van Dongen et al., 2007). Changes in any of sedimentation rate, supply of organic matter, sulfate, reactive iron, and methane can significantly affect hydrogen sulfide generation that in turn, influences the diagenetic alteration of magnetic minerals (Borowski et al., 1996; Dewangan et al., 2013; Kasten et al., 1998, 2003; Riedinger et al., 2005; Roberts, 2015). Rock magnetic investigation has the potential to distinguish between primary magnetic signals from detrital minerals and secondary signals that occur due to diagenetic alteration of primary magnetic minerals in gas hydrate depositional environments. Therefore, rock magnetic techniques can provide important information on different forcing factors (climate, tectonics, sedimentation) that affect gas hydrate formation in marine sediments.

Rock magnetic studies of gas hydrate environments have focused primarily on understanding diagenetic alteration of detrital magnetic minerals (Dewangan et al., 2013; Enkin et al., 2007; Esteban et al., 2008; Johnson & Phillips, 2014; Riedinger et al., 2005; Ski et al., 2017), exploring linkages between magnetic iron sulfides and gas hydrates (Housen & Musgrave, 1996; Kars & Kodama, 2015; Larrasoana et al., 2007; Musgrave et al., 2006), deciphering controls on gas hydrate system evolution (Badesab et al., 2017), rock magnetic properties of gas hydrate bearing sediments (Kars & Kodama, 2015), and developing proxies for tracking paleo-methane seepage events (Novosel et al., 2005; Panieri et al., 2016; Usapkar et al., 2014) and paleo sulfate-methane transition (SMTZ) boundaries (Peketi et al., 2012; Johnson et al., 2014). However, detailed rock magnetic studies that focus on unravelling linkages between sedimentation, shale-tectonism, sediment diagenesis, and gas hydrate formation in marine sedimentary systems are still lacking.

A recent rock magnetic study conducted (Badesab et al., 2017) on a sediment core (NGHP-01-10D) overlying methane hydrate deposits from Krishna-Godavari (K-G) basin examined the sediment magnetic signature of detrital and diagenetic processes associated with evolution of a fracture-filled gas hydrate system. An anomalous magnetic susceptibility zone within gas hydrate bearing intervals at site NGHP-01-10D was reported. However, linkages between magnetic enhancement and gas hydrate formation were poorly resolved. Sediment cores collected during the

first Indian National Gas Hydrate Drilling Expedition (NGHP-Exp-01) record the history of sedimentation, shale tectonics, and geochemical processes that influenced gas hydrate system development in K-G basin (Kumar et al., 2014) and offers an excellent opportunity to obtain a long-term view of magnetic mineral diagenesis in marine gas hydrate sediments. In the present study, we carried out comprehensive rock magnetic measurements complemented by sedimentological analyses of three long sediment cores NGHP-01-03B (299.5m), NGHP-01-05C (194.9 m), and NGHP-01-07B (199.08 m) which provides the longest and most detailed sediment magnetic record available so far from K-G basin. Our work focuses on fingerprinting complex magnetic mineralogical signatures associated with gas hydrate related processes and we present a method for magnetic exploration of gas hydrates in marine sedimentary systems.

## **2. Materials and Methods**

The study area lies on the continental slope of K-G basin (Figure 1), which is a proven petroliferous basin of India (Bastia, 2007). K-G basin is a pericratonic rift basin situated in the central-eastern continental margin of India (ECMI). Sediment thicknesses of 3–5 km in the onshore region and about 8 km in the offshore region have been reported (Bastia, 2007; Prabhakar and Zutshi, 1993). The Krishna and Godavari river systems deliver most of the sediment to this basin. Holocene-Pleistocene sedimentary deposits in the K-G basin are dominated by smectite-bearing Godavari clay formations (Rao, 2001). The estimated annual sediment transport of the Krishna and Godavari rivers is around 67.7 and  $170 \times 10^6$  metric tonnes, respectively (Biksham & Subramanian, 1988; Ramesh & Subramanian, 1988). The presence of subsurface gas hydrate deposits in K-G basin has been confirmed through drilling and sediment coring (Collett et al., 2008). Neo-tectonic activity in K-G basin led to the formation of different types of geomorphic structures on the sea floor, including shale diapirs, faults, and mounds. The fault systems associated with bathymetric mounds facilitate fluid/gas migration and provide favorable sedimentary structures for gas hydrate reservoir formation in K-G basin (Dewangan et al., 2010). The studied core NGHP-01-05C is located on a mound and core NGHP-01-03B is from the slope basin. Core NGHP-01-07B is from close to a submarine channel near Godavari delta.

### **2.1 Sampling and measurements**

The studied sediment cores (NGHP-01-03B, NGHP-01-05C, and NGHP-01-07B) were sub-sampled at 1.5m to 6m intervals. For magnetic analysis, 135 sub-samples were dried, weighed, and packed in 25mm cylindrical sample bottles. Measurements were carried out at the paleomagnetic laboratory of CSIR-National Institute of Oceanography (CSIR-NIO), Goa, India.

## 2.2 Rock magnetic analysis

Low-field magnetic susceptibility measurements were carried out using a Bartington Instruments MS2B dual frequency susceptibility meter. The susceptibility was measured at two (low and high) frequencies  $\chi_{lf} = 0.47$  kHz and  $\chi_{hf} = 4.7$  kHz. The frequency-dependent susceptibility was calculated as  $\chi_{fd} \% = (\chi_{lf} - \chi_{hf}) / \chi_{lf} \times 100\%$ . An anhysteretic remanent magnetization (ARM) was imparted using a 100mT alternating field (AF) with a superimposed fixed direct current (DC) bias field of 50  $\mu$ T, and was measured using a Molspin Minispin spinner magnetometer. Susceptibility of ARM ( $\chi_{ARM}$ ) is calculated as the mass-normalized ARM divided by the DC bias field. An isothermal remanent magnetization (IRM) was imparted in an inducing field of +1 T in the forward direction and was demagnetized by DC backfields at -20 mT, -30 mT, -100 mT, and -300 mT using a MMPM10 pulse magnetizer. The respective remanences were measured using a Molspin Minispin magnetometer. The mass-normalized IRM acquired at a peak field of 1 T is considered to be the saturation IRM (SIRM). S-ratio is calculated as the ratio between the IRM at -300 mT and SIRM ( $IRM_{-300mT}/SIRM_{1T}$ ) (Thompson & Oldfield, 1986). Temperature-dependent magnetic susceptibility ( $\chi-T$ ) measurements on fifteen selected samples were carried out at the Indian Institute of Geomagnetism (IIG) in a 300 A/m field at 875 Hz with a CS-3 furnace coupled to an Agico (KLY-4S) Kappabridge system. High-temperature measurements were performed from room temperature to 700°C in an argon atmosphere. Hysteresis loops, first order reversal curves (FORC) (Pike et al., 1999), and back-field demagnetization curves were also measured for twenty-two selected samples with a saturating field of 1 T (field increment of 4 mT, averaging time of 200 ms, and a slew rate limit of 1 T/s) at the Center for Advanced Marine Core Research (CMCR), Kochi University, Japan. FORC diagrams were processed using the FORCinel software (Harrison & Feinberg, 2008).

Low-temperature magnetic measurements were performed at the (CMCR). A Quantum Design Magnetic Properties Measurement System (MPMS) was used for remanence measurements on representative samples covering the four sediment zones of cores NGHP-01-05C and NGHP-01-07B. A RT-SIRM was imparted at room temperature (300 K) with a 2.5 T. Samples were then cooled to 5 K and warmed back to 300 K in a zero magnetic field. A LT-SIRM was then imparted at 5 K with a 2.5 T. Samples were warmed up to 300 K in a zero magnetic field (termed "ZFC" for zero field-cooled). Samples were then cooled to 5 K in the presence of a 2.5 T magnetic field. A LT-SIRM was again imparted at 5 K and samples were warmed to 300 K in a zero magnetic field (termed "FC" for field-cooled). Magnetic parameters were normalized by sample mass.  $\delta_{FC}$  and  $\delta_{ZFC}$  were calculated

following Moskowitz et al. (1993) to differentiate the origin of magnetite (biogenic or inorganic).  $\delta$  is a measure of the amount of remanence lost during warming through the Verwey transition.

## **2.3 Sedimentological analyses**

### **2.3.1 Grain size measurements**

Sediment grain size measurements were carried out using a Malvern Mastersizer 2000 Laser Particle Size Analyzer at CSIR-NIO. Sediment samples were first desalinated and were later decarbonated using dilute HCl (1 N). Sediment suspensions were treated with 10% H<sub>2</sub>O<sub>2</sub> to remove organic carbon and the dispersing agent Na-hexametaphosphate was added to the suspension, which was then ultrasonicated prior to analysis. Grain size values are presented as volume %.

### **2.3.2 Mineralogical analysis**

Magnetic particles were separated from the bulk sediment following the extraction method of Petersen et al. (1986). Images of magnetic particles were captured in secondary electron (SE) imaging mode at energy levels between 15 and 20 keV using a scanning electron microscope (SEM) (JEOL JSM-5800 LV). The composition of magnetic particles was determined using an energy dispersive X-ray spectroscopy (EDS) probe attached to the microscope. The magnetic mineralogy of representative samples from all three sediment cores was determined using a Rigaku X-Ray Diffractometer (Ultima IV). The samples were run from 15° to 70° of 2 $\theta$  at 1°/min scan speed using Cu K $\alpha$  radiation ( $\lambda = 1.5414 \text{ \AA}$ ).

## **2.4 Geochemical analyses**

Chromium reducible sulfur (CRS) contents of the studied sediment cores (MD161/Stn8, MD161/Stn13, NGHP-01-10D) were made following Peketi et al. (2012, 2015). Pore water sulfate and methane data for the sediment cores (NGHP-01-10D, NGHP-01-03B, NGHP-01-05C, and NGHP-01-07B) are presented in Figure S3. These data are from Collet et al. (2008).

## **2.5 Geophysical Data**

High-resolution seismic (HRS) data for sites NGHP-01-10D, NGHP-01-03B, and NGHP-01-05C are from Ramprasad et al. (2011) and Anitha et al. (2014). An interpreted seismic section is shown in Figure S2.

## **3. Results**

### **3.1 Down-core rock magnetic property variations**

Based on down-core magnetic property changes in sediment cores NGHP-01-03B, NGHP-01-05C, and NGHP-01-07B, four sediment zones (Z-I, Z-II, Z-III, and Z-IV) are identified (Figures 3a-3o). A largely uniform and extended thickness of enhanced magnetic susceptibility is present in all four sediment cores (Figures 2a-2d). The topmost zone (Z-I) of cores NGHP-01-03B, NGHP-01-05C, and NGHP-01-07B contains a decreasing  $\chi_{lf}$  and SIRM trend, which suggests down-core reduction in magnetic mineral concentration (Figures 3a, 3b, 3f, 3g, 3k, and 3l). The lower ARM/SIRM and higher S-ratio (0.90 – 1.0) in NGHP-01-03B and NGHP-01-05C reflect the dominance of coarse-grained magnetite in this zone (Figures 3c, 3d, 3h, and 3i), while higher ARM/SIRM in NGHP-01-07B indicates the presence of fine-grained magnetic particles (Figure 3m). A noticeable decrease in concentration of magnetic minerals is observed in Z-II as reflected by low  $\chi_{lf}$  and SIRM values (Figures 2a, 2b, 2c, 2d, 3f, 3g, 3k, and 3l). Z-III is marked by a sudden increase in magnetic mineral concentration as reflected in  $\chi_{lf}$  and SIRM (Figures 3a, 3b, 3f, 3g, 3k, and 3l). Higher S-ratios suggest the predominance of ferrimagnetic minerals in this zone (Figures, 3d, 3i, and 3n). A substantial drop in  $\chi_{lf}$  and SIRM coincides with the depth of the BSR in core NGHP-01-05C (Figure 3f-3g). A similar drop in  $\chi_{lf}$ , SIRM, and S-ratio is observed below the present day BSR in NGHP-01-03B and well above in NGHP-01-07B (Figures 3a, 3b, 3d, 3k, 3l, and 3n). Within Z-III, a few minor  $\chi_{lf}$  drops are also evident (Figures 3a, 3f, and 3k). A minor increase in  $\chi_{lf}$  and SIRM occurs in Z-IV of NGHP-01-05C and NGHP-01-07B, while an opposite trend is observed in NGHP-01-03B (Figures 3a, 3b, 3f, 3g, 3k, and 3l). A pronounced ARM/SIRM increase in Z-IV of NGHP-01-03B reflects a finer magnetic mineral grain size (Figure 3c). A notable sediment grain size increase is seen in Z-III of cores NGHP-01-05C and NGHP-01-07B, while no distinct trend occurs in cores NGHP-01-03B (Figures 3e, 3j, and 3o).

## 3.2 Magnetic mineralogical and granulometric proxies

### 3.2.1 Temperature-dependent magnetic susceptibility

$\chi$ -T curves of representative samples from Z-I, Z-II, Z-III, and Z-IV of cores NGHP-01-03B, NGHP-01-05C, and NGHP-01-07B are shown in Figure 4. A sharp magnetic susceptibility decrease between 570°C and 600°C suggests that the bulk magnetic mineralogy is dominated by magnetite (Dunlop & Özdemir, 1997) (Figures 4a - 4l). The  $\chi$  increase between 300°C and 500°C is likely due to conversion of paramagnetic minerals such as pyrite and iron-bearing silicates, iron-rich carbonates, siderite and iron-rich smectites into magnetite during heating (Cui et al., 2017; Hirt et al., 1993; Hirt & Gehring, 1991; Pan et al., 2000; Passier et al., 2001; Phillips, 2018) (Figures 4a-4l).

### 3.2.2 Low-temperature magnetometry

Low-temperature measurements for representative samples from different magnetic zones of cores NGHP-01-05C and NGHP-01-07B are characteristic of the different magnetic minerals present in the studied samples (Figure 5). For samples from Z-I, a Verwey transition due to detrital magnetite ( $T_v$  118 - 120 K) is evident in RT-SIRM, in first derivative of magnetization curves and the remanence did not recover fully during warming (Figures 5a-5d) (Chang et al., 2016a; Muxworthy & McClelland, 2000; Özdemir et al., 2002; Verwey, 1939). Samples from the magnetically reduced zone (Z-II) of core NGHP-01-05C do not provide evidence of a Verwey transition in RT-SIRM, ZFC-FC, and first derivative of magnetization curves (Figures 5e-5f). Nearly 60% of the LT-SIRM imparted at 5 K is lost during warming between 5 and 35 K (Figures 5e-5f). This indicates the presence of superparamagnetic (SP) magnetic particles (Passier & Dekkers, 2002; Tarduno et al., 1995). It is highly likely that the SP magnetic particles are greigite because fine magnetite particles would dissolve in sulfidic settings, while SP greigite nanoparticles would be thermodynamically more stable in contrast to SP magnetite nanoparticles (Rowan et al., 2009; Roberts et al., 2018). Samples from the same zone (Z-II) of core NGHP-01-07B have a Verwey transition at ~ 120 K in the RT-SIRM and first derivative of magnetization curves which indicates the presence of detrital magnetite (Chang et al., 2016a, Figure 5g-5h). Samples from the magnetically enhanced zone (Z-III) of core NGHP-01-07B has a well-developed Verwey transition in RT-SIRM and first derivative of magnetization curves (Figure 5k-5l). The remanence does not recover totally during warming of RT-SIRM. In the same zone (Z-III) of NGHP-01-05C, the Besnus transition at ~35 K is typical of detrital pyrrhotite as evident in the RT-SIRM cooling and first derivative of magnetization curves (Dekkers, 1989; Horng & Roberts, 2006; Rochette et al., 1990) (Figures 5i-5j), but lack of such a transition is not diagnostic of authigenic pyrrhotite, which lacks a low-temperature transition (Horng & Roberts, 2018). The remanence recovers totally during warming of the RT-SIRM, which suggests the occurrence of single domain (SD) pyrrhotite. We did not observe any typical pyrrhotite features in the ZFC-FC curves. Higher  $T_v$  value in the samples from Z-I and Z-III are indicative of detrital magnetite (Chang et al., 2016a) (Figures 5b, 5d, 5j, and 5l). Below the present day BSR, i.e., Z-IV, magnetic characteristics are similar to those of Z-II (Figures 5e, 5f, 5m, 5n, 5o, and 5p). The Verwey transition is nearly absent and no transitions are evident in the ZFC-FC curves (Figures 5n and 5p). No LT transition has been observed in magnetization derivative curves in Z-II and Z-IV samples, which is consistent with the presence of greigite (Figures 5f, 5n, and 5p) (Chang et al., 2009; Roberts et al. 2011).



### 3.2.3 FORC diagrams

In addition to diagnostic room- and low-temperature magnetic measurements, FORC diagrams were obtained to provide information about magnetic minerals and domain states of samples from cores NGHP-01-05C and NGHP-01-07B. Representative FORC diagrams for the four sediment zones of cores NGHP-01-05C and NGHP-01-07B are shown in Figures 6a-6h. FORC distributions for most of the samples are characterized by a peak at  $B_C \sim 10$  mT with closed contours that are indicative of the dominance of vortex state behavior in magnetite (Lascu et al., 2018; Muxworthy & Dunlop, 2002; Roberts et al., 2000; Roberts et al., 2017) (Figure 6a-6h). FORC distributions for samples from Z-IV (i.e., at BSR depth) of cores NGHP-01-05C and NGHP-01-07B are also indicative of vortex state ( $B_C \sim 10 - 15$  mT) magnetite (Figures 6g-6h).

### 3.3 Mineralogical analyses of magnetic particles

SEM-EDS analyses support our rock magnetic observations and confirm that titanomagnetite is the dominant magnetic mineral in the studied sediments. Detrital ferrimagnetic iron oxides and diagenetic magnetic iron sulfide minerals of various sizes are observed in all sediment cores (Figures 7a-7l). Z-I contains well-preserved, fresh and relatively less altered titanomagnetite grains. EDS data for these grains indicate the presence of iron, titanium, and oxygen with minor traces of silicon, calcium, potassium, manganese, aluminum, and vanadium (Figures 7a, 7e, and 7i). Diagenetically formed pyrite crystals occur as individual grains and as aggregates in the magnetically weak zone (Z-II). EDS data indicate the presence of sulfur and iron along with minor amounts of calcium, phosphorous, aluminium, and silicon (Figures 7b, 7f, and 7j).

In magnetically enhanced zone (Z-III), we observed numerous titanomagnetite and pyrite grains with various sizes and shapes. The titanomagnetite grains showed evidence of corrosion related to diagenetic alteration (Figures 7c, 7g, and 7k). EDS data indicate a dominance of iron, titanium, and sulfur with traces of phosphorous, calcium, silicon, potassium, and manganese (Figures 7c, 7g, and 7k). In addition to discrete Fe-Ti rich magnetic particles, numerous titanohematite particles with pyrite growths were found in this zone. Skeletal titanohematite lamellae (Figure S1a), pyrite overgrowths on titanomagnetite grains (Figure S1b), and well-preserved titanomagnetite grains are observed (Figure S1c). Z-IV (i.e., below the present-day BSR) contains a mixture of titanomagnetite and pyrite grains (Figures 7d, 7h, and 7l). EDS results reveal the presence of sulfur, iron, and titanium with minor traces of calcium, silicon, aluminum, and manganese (Figures 7d, 7h, and 7l).

### 3.4 X-ray diffraction (XRD) analysis on magnetic separates

Titanomagnetite is also identified in XRD results as the dominant magnetic mineral in all sediment zones (Figures 8). XRD data confirm the presence of pyrite in zones with reduced magnetic susceptibility (Z-II and Z-IV) (Figures 8b, 8d, 8f, 8h, 8j, and 7l). Pyrite is also present in the magnetically enhanced zone (Z-III) in all three studied sediment cores (NGHP-01-03B, NGHP-01-05C, and NGHP-01-07B) (Figures 8c, 8g, and 8k).

### 3.5 Correlation between magnetic and geochemical parameters

As previously documented by Badesab et al. (2017) in core NGHP-01-10D, a positive relationship between  $\chi_{lf}$  and SIRM is observed in all analyzed cores, but with different slopes for different mineral types (Figure 9a). Two distinct groupings are evident. Samples from core NGHP-01-07B have higher  $\chi_{lf}$  and low SIRM compared to cores NGHP-01-03B and NGHP-01-05C which have linear relationships between  $\chi_{lf}$  and SIRM (Figure 9a). Magnetite concentration ( $\chi_{lf}$ ) variations are large, while high  $\chi_{lf}$  and lower  $\chi_{fd}\%$  values suggest the dominance of coarser magnetic grains (Figure 9b).  $\chi_{fd}$  largely varies from 0 to ~ 6% (Figure 9b). Lower values for some samples that have higher  $\chi_{fd}$  value reflects a finer grain size trend for a subset of the data (Figure 9b).

SIRM/ $\chi_{lf}$  versus  $\chi_{lf}$  trends have proven to be diagnostic of identifying different magnetic mineral types in gas hydrate bearing sediments (Larrasoana et al., 2007). The analyzed samples are categorized into three subgroups (Figure 9c). Samples with low SIRM/ $\chi_{lf}$  and higher  $\chi_{lf}$  values indicate the dominance of magnetite. Lower  $\chi_{lf}$  and wide- ranging SIRM/ $\chi_{lf}$  values suggest the presence of ferrimagnetic iron sulfides. Data that fall within the intermediate range of  $\chi_{lf}$  and SIRM/ $\chi_{lf}$  values represent mixtures of magnetite and magnetic iron sulfides (Figure 9c).

As indicated above, the bulk magnetic mineralogy is dominated by vortex state titanomagnetite. The source of magnetic mineral assemblages can be differentiated by  $\delta_{ZFC}$  and  $\delta_{FC}$  as proposed by Moskowitz et al. (1993).  $\delta_{FC}/\delta_{ZFC}$  values are close to 1, which indicates that the titanomagnetites are detrital (Figure 9d) (Moskowitz et al., 1993; Housen & Moskowitz, 2006). All data cluster according to mineralogy and fall on a 1:1 line. Samples with low  $\delta_{ZFC}$  and  $\delta_{FC}$  (<0.18) represent the ferrimagnetic iron sulfides, while high  $\delta_{ZFC}$  and  $\delta_{FC}$  values (>0.4) correspond to magnetite (Figure 9d) (Kars & Kodama, 2015).

Negative correlation between  $\chi_{lf}$  and CRS is observed for cores MD161/Stn8, MD161/Stn13, and NGHP-01-10D, which lie near cores NGHP-01-03B and NGHP-01-05C from this study and overlie methane hydrate deposits from K-G basin (Figures 1, and 9e). A clear trend of reducing  $\chi_{lf}$

with increasing CRS is suggested here to be a proxy for identifying the paleo-methane seepage events in gas hydrate forming environments as documented by Badesab et al. (2017).

#### 4. Discussion

We examined the magnetic and sedimentological signatures of three sediment cores to evaluate the influence of sedimentary, tectonic, and diagenetic processes on the development of a fracture-filled gas hydrate system in K-G basin. We explore these influences below.

##### 4.1 Controls on supply of magnetic minerals to K-G Basin.

Changes in monsoons, Himalayan uplift, weathering intensities, erosional processes in peninsular India, and glacial/interglacial cycles influenced the supply of detrital particles to K-G basin (Curry et al., 1982; Collins et al., 1999; Krishna et al., 2016; Rao and Kessarkar, 2001; Sangode et al., 2001; Weber et al., 1997). The K-G basin receives a large sediment load from peninsular India through the Krishna and Godavari rivers. These rivers drain through the Deccan Traps basalts and Precambrian metamorphic rocks and deliver sediments from these terrains into K-G basin (Ramesh and Subramanian, 1988). Sediment cores NGHP-01-10D, NGHP-01-03B, NGHP-01-05C, and NGHP-01-07B from K-G basin preserve a record of sedimentary processes in the basin. Down-core magnetic property and sediment grain size variations are interpreted to indicate different controls on magnetic mineral supply into K-G basin. Almost uniform and enhanced magnetic susceptibilities in Z-III in all studied cores may be attributed to multiple MTDs as observed in K-G basin (Figures 2a-2d, Figures 3a-3o, and Figure S2). Titanomagnetite is the most abundant magnetic mineral in Deccan basalts (Sangode et al., 2001) and fluvial sediments from peninsular India. The Krishna and Godavari Rivers have much higher magnetite contents compared to those sourced from Himalayan regions (Sager & Hall, 1990; Phillips et al., 2014b; Prajith et al., 2018; Sangode et al., 2001, 2007). Magnetic, XRD and SEM results indicate the dominance of well-preserved coarse titanomagnetite grains in zone-III (Figures 3a-3o, Figures 4g-4i, Figures 5i-5l, Figures 7c, 7g, and 7k, Figures 8c, 8g, and 8k). These observations suggest that detrital magnetic particles in Z-III are sourced from Deccan basalts and were mainly supplied during periods of high sedimentation through peninsular river systems.  $\chi_{lf}$  fluctuations within Z-III provide indications of multiple short-term higher sedimentation events in K-G basin (Figures 2a-2d, 3a, 3f, and 3k, and Figure S2). They also indicate that in the rapidly depositing sedimentary system of K-G basin, magnetic susceptibility scanning of sediment cores has the potential to detect subtle variations in detrital sediment inputs into marine basins.

Mass transport deposits (MTDs) are found commonly on the continental slopes, in channel–levee systems, and in basin-floor settings, for example, in Kumano Basin, Nankai Trough, Japan, the West African margin, North Sea, Gulf of Mexico, and the Californian and Brazilian margins (Moore et al., 2016; Shanmugam et al., 1994, 1995; Shanmugam, 2006). In K-G basin, multiple MTDs have been identified in shallow (Ramana et al., 2007; Ramprasad et al., 2011) and deep offshore regions (Yamamoto et al., 2018), as confirmed by high-resolution seismic reflection data, multibeam bathymetry, seafloor topography, physical properties, lithology and sediment ages (Ramprasad et al., 2011; Yamamoto et al., 2018). Recent studies demonstrate that neo-tectonic events, gas hydrate dissociation, sea level variations, and rapid sedimentation events can trigger slumping/sliding to produce MTDs in K-G basin (Ramana et al., 2007, Ramprasad et al., 2011). High-resolution seismic records of sites NGHP-01-10D, NGHP-01-03B, and NGHP-01-05C indicate the presence of multiple acoustically transparent layers with no internal reflections that are typical of MTDs and indicate that the deposits are formed instantaneously (Figure S2) (Anitha et al., 2014; Pratson and Laine, 1989; Ramprasad et al., 2011). The sub-bottom profiler data from K-G basin indicate the occurrence of Holocene and pre-Holocene MTDs which are overlain by finely-layered sediments (Dewangan et al., 2011; Mazumdar et al., 2012; Ramana et al., 2007; Ramprasad et al., 2011). A distinct band of enhanced magnetic susceptibility (Z-III) in core NGHP-01-10D reported by Badesab et al. (2017) appears to be a larger extensive feature throughout K-G basin as seen in cores NGHP-01-05C and NGHP-01-07B (Figures 2a-2d). Mazumdar et al. (2012) provided a direct indication for slumping and mass transportation of deposits as evident by the age reversal in  $^{14}\text{C}$  AMS dates observed in sediment cores from K-G basin. We propose that the magnetically enhanced and laterally extensive band of Z-III observed in all four cores represents several MTDs that may have been generated by more rapid sedimentation events in slope regions of K-G basin that were later buried to form a distinct and magnetically enhanced sediment magnetic property zone (Z-III) as evident at all four sediment cores (Figures 2a-2d, 3a, 3f, and 3k, Figure S2). Such repeated MTDs contributed to produce an overall higher sedimentation rate interval in K-G basin.

#### 4.2 Linkages between shale-tectonics, high sedimentation events, and gas hydrate formation in the K-G basin

Gravity-driven shale tectonics governs the formation of shale bulges and toe-thrust structures in K-G basin (Choudhuri et al., 2010), which host major gas hydrate deposits (Dewangan et al., 2010). The spatial and temporal distribution of these structures depends on tectonic events and sediment depocenters in the basin over geological timescales. Rapid deposition of Miocene

sediments after establishment of the monsoon system at ~24 Myr (Clift et al., 2008) led to formation of over-pressured shale strata in K-G basin. The movement of mobile shale strata resulted in numerous growth faults in the upper shelf and upper slope regions with proximal and distal shale bulges in the middle slope and rise regions (Choudhuri et al., 2010). The proximal shale bulges continued to grow during the Pliocene due to ongoing sedimentation in the shelf region while distal bulges ceased to grow during this period. Increased sediment flux at 0.8 Ma due to increased deformation in the Himalayas (Clift et al., 2005) led to formation of mega depocenters in the shelf region (Krishna et al., 2016). We propose that this increased late Pleistocene sedimentation might have accentuated shale bulge growth, which appear as bathymetric mounds on the seafloor. These mounds are potential locations for gas hydrate formation (Dewangan et al., 2010).

We now attempt to link magnetic properties with neotectonic events in K-G basin. Magnetic minerals supply, transportation, and burial in marine sediments are controlled by climatic, tectonic, and hydrodynamic forcing and hence,  $\chi_{lf}$  variations can provide clues about sedimentary processes and depositional environments (Hatfield & Maher, 2008, 2009; Oldfield et al., 1985). In K-G basin, shale tectonism has led to the development of faults, fractures, mounds, and ridges on the seafloor. Sediment cores NGHP-01-10D and NGHP-01-5C lie on a mound and the observed magnetically enhanced Z-III in both cores appears to represent the former shale bulges that formed as a result of shale strata movement (Figure 2) (Choudhuri et al., 2010; Dewangan et al., 2010).

Later, as sedimentation increased during the Pleistocene, this region was exposed to rapid uplift and faulting as a result of shale-tectonism that was triggered by rapid sediment loading (Dewangan et al., 2010; Krishna et al., 2016). Highly pressurized strata were generated as a result of higher sedimentation rates that triggered growth of faults, folds, and upthrusting features (bathymetric mounds, ridges) in K-G basin. These structures likely acted as conduits for upward fluid/gas migration to enter the gas hydrate stability zone (Dewangan et al., 2010; Shankar & Riedel, 2010). A five-fold late Pleistocene sedimentation rate increase in K-G basin (Krishna et al., 2016) led to generation of large MTDs that were deposited rapidly and provided the pressure and temperature conditions needed for gas hydrate nucleation (Figure S2). The highest gas hydrate saturations occur within magnetically enhanced Z-III in all studied cores (Figure 3) (Collet et al., 2014; Kumar et al., 2014). Fault growth facilitated methane gas migration through magnetically enhanced Z-III, which led to formation of huge gas hydrate deposits. Therefore, observed magnetic property variations at the studied sites (NGHP-01-10D, NGHP-01-05C) are controlled largely by episodic flow of methane and sulfide-enriched fluids through the fracture network that formed as a result of shale-tectonism.

During periods of normal sedimentation (Z-II), gas hydrate accumulation along the fault system resulted in fault system closure (Badesab et al., 2017).

More rapid sedimentation and tectonic stress could increase significantly the pore-fluid pressure of highly pressurized strata leading to fluid migration to shallower depths (Flemings et al., 2006, 2008; Yamamoto et al. 2007, 2009; Yamamoto & Kawakami, 2014). Increased pore pressure beyond the sediment shear strength could trigger methane-rich fluid expulsion/seepage events (Cremiere et al., 2016; Karstens et al., 2018). Episodic methane seepage would lead to multiple events of AOM-coupled sulfate reduction to cause dissolution of primary magnetic mineral assemblages and precipitation of secondary magnetic iron sulfides to create a distinct sediment magnetic signature (Dewangan et al., 2013; Riedinger et al., 2005). A sudden  $\chi_{\text{f}}$  drop due to iron oxide dissolution and pyrite growth and enriched CRS within Z-III (Peketi et al., 2012) provide clues of multiple past methane seepage events triggered by short-term paleo-methane expulsion events in K-G basin similar to those observed in the continental margin offshore of Argentina and Uruguay (Riedinger et al., 2005). Previous multi-proxy studies by Mazumdar et al. (2009) confirmed the occurrence of paleo-methane expulsion events at sites MD161/Stn 8 and MD161/Stn 13 (close to site-NGHP-01-10D). Hence, it is likely that shale-tectonism induced by rapid sedimentation events played a key role in evolution of the K-G basin gas hydrate system.

Differential sediment loading due to a Pliocene change in the direction and amount of sediment supply in the Bay of Bengal was driven by climatic and tectonic changes and resulted in a shift of sediment depocentres in K-G basin (Choudhuri et al., 2010; Cullen., 1981; Prell et al., 1980; Sangode et al., 2007). Core NGHP-01-03B is located in a marginal slope basin that formed during recent shale bulge uplift, and has low  $\chi_{\text{f}}$  and SIRM unlike cores NGHP-01-05C and NGHP-01-07B (Figures 2b, 3a and 3b). We propose that core NGHP-01-03B was formerly a sediment depocenter dominated by mixed, poorly-sorted, and weakly magnetic sediments as reflected by relatively low  $\chi_{\text{f}}$  and mixed sediment grain size in Z-III as compared to other cores NGHP-01-05C and NGHP-01-07B (Figures 3a, 3b, and 3e).

#### 4.3 Diagenetic alteration of detrital magnetic minerals

Down-core variations in magnetic mineral concentration, grain size, and mineralogy in all studied cores seem to be largely affected by the identified rapid sedimentation events and by post-depositional sediment diagenesis induced by AOM-coupled sulfate reduction processes (Figures S2, and S3). Reduction of  $\chi_{\text{f}}$  with depth in Z-I is attributed to diagenetic transformation that resulted in primary detrital iron oxide dissolution and iron sulfide precipitation (Figures 2a-2d, 3a, 3f, and 3k,

4a-4c, 7a, 7e, and 7i, 8a, 8e, and 8i). A  $\chi_{\text{fr}}$  decrease and the presence of pyrite within the sulfidic zone (Z-II), i.e., the present depth of the SMTZ, are due to pyritization fuelled by enhanced AOM-coupled sulfate reduction (Figures 2a-2d, 7b, 7f, 7j, 8b, 8f, 8j, and S3). Increased sedimentation in K-G basin during sediment interval Z-III affected diagenetic processes and favored rapid burial to cause less alteration and enhanced preservation of detrital magnetic particles to create a magnetically enriched interval Z-III (Figure S2). Skeletal titanohematite grains in Z-III are indicative of diagenetic dissolution of the Fe-rich parts of the particle (Nowaczyk 2011; Roberts, 2015) with Ti-rich parts being less reactive (Figure S1a). Higher  $T_v$  values in samples from Z-I and Z-III indicate the presence of detrital magnetite (Figures 5a-5d and 5i-5l) (Chang et al., 2016a). Z-IV lies below the present-day BSR and is marked by low  $\chi_{\text{fr}}$  with the presence of magnetic iron sulfides that might have formed as a result of deep pyritization processes and that probably represent a fossil gas hydrate sedimentary interval as proposed by Badesab et al. (2017) (Figures 7h and 7l, 8d and 8l). This interpretation is similar to findings at Nankai Trough (Kars & Kodama, 2015a, 2015b), and Cascadia Margin (Housen & Musgrave, 1996; Larrasoña et al., 2007).

Previous studies have reported the widespread occurrence of the magnetic iron sulfides, greigite ( $\text{Fe}_3\text{S}_4$ ) and hexagonal pyrrhotite which formed authigenically in methane-rich and gas hydrate bearing sedimentary environments at Hydrate Ridge, Cascadia Margin (Housen & Musgrave, 1996; Larrasoña et al., 2007; Musgrave et al., 2006), Nankai Trough (Kars & Kodama, 2015a, 2015b) and the continental margin offshore of southwestern, Taiwan (Horng, 2018; Horng & Roberts, 2018). The presence of gas hydrates enhances microbial activity that results mainly in ferrimagnetic greigite precipitation (Housen & Musgrave, 1996; Riedinger & Brunner, 2014). Microbiological studies by Cragg et al. (1996) in sediment cores from Cascadia margin observed that methane oxidation rates are enhanced within the gas hydrate zone and results in increased bacterial populations. The availability of methane to fuel microbiological activity during gas hydrate formation, lead to iron sulfide precipitation from brine with high concentration of sulfide (Wellsbury et al., 2000). Larrasoña et al. (2007) reported that in southern Hydrate Ridge, authigenic greigite and pyrrhotite formed as a by-product of microbially-mediated diagenetic reactions in the AOM, and gas hydrate zone. We did not observe greigite here in the potential gas-hydrate bearing sedimentary zone (Z-III, Z-IV). Dewangan et al. (2013) reported greigite in Z-II (17-23 mbsf) of a sediment core (MD161/Stn 8) close to core NGHP-01-10D. It is possible that greigite was formerly present in Z-II, Z-III, and Z-IV in the studied cores. Later, when conditions became disadvantageous for greigite formation/preservation due to gas hydrate dissociation caused by changing pressure-temperature or increased sedimentation (Housen & Musgrave, 1996; Karsten et al., 2018; Larrasoña et al., 2007;

Musgrave et al., 2006), ferrimagnetic greigite would have been subsequently transformed into paramagnetic pyrite in Z-II, Z-III, and Z-IV (Berner, 1984; Kao et al., 2004). Similar observations have been reported for a sediment core (Hole C0008C) from the megasplay fault zone of Nankai Trough (Kars & Kodama, 2015). As evident from XRD data, the presence of pyrite within magnetic mineral extracts from Z-II, Z-III, and Z-IV could also be due to the occurrence of particles with a pyrite rim and greigite core (Figures 8b, 8c, 8d, 8f, 8g, 8j, 8k, and 8l) (Ebert et al., 2018; Roberts & Turner, 1993). The common presence of quartz in magnetic mineral extracts from all zones could also be due to silicate-hosted magnetic mineral inclusions that are protected and survive diagenetic dissolution (Chang et al., 2016b) (Figure 8).

The presence of pyrrhotite has been reported widely in methane-rich sedimentary environments where high concentration of methane occur near disseminated gas hydrates (Jørgensen et al., 2004; Kars & Kodama, 2015a, 2015b; Larrasoña et al., 2007; Neretin et al., 2004; Roberts et al., 2010). Hexagonal pyrrhotite ( $\text{Fe}_9\text{S}_{10}$  or  $\text{Fe}_{11}\text{S}_{12}$ ) often forms authigenically in methanic sedimentary environments (Horng, 2018), while monoclinic pyrrhotite (ferrimagnetic) ( $\text{Fe}_7\text{S}_8$ ) is found widely in igneous and metamorphic rocks (Horng & Roberts, 2006; Horng et al., 2012; Horng & Huh, 2011; O'Reilly et al., 2000; Rochette et al., 2001, 2003) and can be eroded and transported through river systems to be deposited in marine environments. Low-temperature magnetic data indicate the presence of monoclinic pyrrhotite based on the presence of the Besnus transition at  $\sim 35$  K in Z-III of core NGHP-01-05C (Figures 5i-5j). Horng & Roberts (2018) argued that detrital monoclinic pyrrhotite grains released from proximal sources (igneous or metamorphic sources) will exhibit a Besnus transition, while hexagonal pyrrhotite that is observed widely in methane-rich sediments offshore of southwestern Taiwan does not exhibit a Besnus transition. Deccan basalts and Precambrian metamorphic rocks in the hinterlands surrounding K-G basin are potential sources of detrital pyrrhotite in the studied samples (Ramesh & Subramanian, 1988). Clay mineralogical studies have demonstrated that the peninsular rivers are the major supplier of sediments to K-G basin (Mazumdar et al., 2015; Rao et al., 1988; Rao, 1991). Hence, the monoclinic pyrrhotite identified in the much wider gas hydrate bearing sediment magneto zone (Z-III) of Hole-NGHP-01-05C (Figures 5i-5j) interpreted to have a detrital origin. The absence of LT transitions in magnetically reduced Z-II and Z-IV is consistent with the presence of iron sulfides (greigite, hexagonal pyrrhotite), which are commonly present in such methane-rich environments and does not exhibit a LT transition. In such cases, LT magnetic results do not provide clear magnetic mineral identifications, so other methods are needed to detect such minerals (Chang et al., 2009; Roberts et al., 2011) (Figures 5f, 5n, and 5p).



#### 4.4 Magnetic susceptibility as a proxy for tracking paleo sulfate-methane transition zones (SMTZ) and methane seepage events in marine sediments

Past studies have demonstrated the potential of  $\chi_{lf}$  as a proxy for identifying the SMTZ in continental margin sediments offshore of Argentina and Uruguay (Riedinger et al., 2005), southwestern Taiwan (Horng & Chen, 2006), rapidly deposited sediments offshore of North Island, New Zealand (Rowan & Roberts, 2006), coal-bearing sediments, offshore of Shimokita Peninsula, Japan (Phillips et al., 2017), the Argentine continental slope (Garming et al., 2005), Nankai Margin, southwestern Japan (Kars & Kodama, 2015a, 2015b; Shi et al., 2017), Cascadia margin offshore of western North America (Housen & Musgrave, 1996; Larrasoana et al., 2007), and Vestnesa Ridge, offshore of western Svalbard (Schneider et al., 2018; Szybor & Rasmussen, 2017a). Effects of higher sedimentation rates and sedimentary events (e.g., mass transport deposits) on the sediment geochemical record, especially for reconstructing past methane seepage events is not well understood. K-G basin is characterized by dynamic depositional conditions controlled by non-steady-state sedimentary processes (abrupt sedimentation changes), sub-surface gas hydrate occurrence, paleo-methane seepage events, sediment slumping/sliding, MTDs, and fault system growth induced by shale-tectonics. Therefore, K-G basin provides a suitable sedimentary environment to test the potential of magnetic susceptibility as a proxy for tracking paleo-SMTZ fronts in a complex marine sedimentary system (Dewangan et al., 2010; Mazumdar et al., 2009; Peketi et al., 2012, Ramana et al., 2009; Ramprasad et al., 2011; Shanmugam et al., 2009; Shankar & Riedel, 2010). A drop in  $\chi_{lf}$  and SIRM, and the presence of pyrite within the sulfidic zone (Z-II) are attributed to intense pyritization fuelled by AOM-coupled sulfate reduction at the present-day SMTZ (Figures 3a, 3f, 3k, 7b, 7f, and 7j, 8b, 8f, 8j, and S3) (Collet et al., 2008). Maintaining the SMTZ at specific sediment depths is governed by the upward-migrating methane flux, downward diffusion of sulfate, and sedimentation variations. In the AOM zone, the rate of  $\chi_{lf}$  loss is determined by the contact time between iron-bearing minerals and reactive  $H_2S$ -rich fluids (Canfield & Berner, 1987; Canfield, 1992; Dewangan et al., 2013; Riedinger et al., 2005; Roberts & Turner, 1993). MTDs generated by rapid sedimentation events could significantly alter  $H_2S$  build-up at the SMTZ front and thereby reduce the contact time required for completion of diagenetic reactions that result in partial magnetic susceptibility loss as documented from the continental margin offshore of Argentina and Uruguay (Riedinger et al., 2005), and Krishna-Godavari Basin (Badesab et al., 2017; Dewangan et al., 2013; Hong et al., 2014b). The anomalous  $\chi_{lf}$  increase and coarsening of magnetic grain size in Z-III of cores NGHP-01-10D, NGHP-01-03B, NGHP-01-05C, and NGHP-01-07B has been attributed to

MTD complexes generated by higher sedimentation events in K-G Basin (Figure 3 and Figure S2). Distinct  $\chi_{lf}$  drops at several depth intervals followed by the occurrence of pyrite and titanomagnetite grains within Z-III, i.e., below the present-day SMTZ, provide clues about the temporal build-up and rapid migration of paleo-SMTZ fronts that were caused by short-lived AOM-coupled sulfate reduction activity affected by abrupt sedimentation (Figure 3 and Figure S2). The intermitted occurrence of lower  $\chi_{lf}$  within Z-III also hints at periods of decreased sedimentation rate that favored partial iron mineral dissolution through weakened pyritization. Therefore, it is likely that in the rapidly depositing K-G basin sedimentary system, sufficient methane concentrations and lower sedimentation rates are required for long-term sustenance of the SMTZ, which eventually created distinct  $\chi_{lf}$  minima. However, in such a scenario, magnetic tracking could help to resolve subtle changes caused by short-term fluctuations in sediment supply and diagenesis.

Recent studies have demonstrated that in rapidly depositing methane-rich marine sedimentary environments, enrichment of CRS ( $\delta^{34}\text{S}_{\text{CRS}}$ ) and molybdenum (Mo) can be used as proxies to identify paleo-SMTZs and methane seepage events in marine sediments (Chen et al., 2016; Hu et al., 2017; Li et al., 2016; Lin et al., 2016; Peketi et al., 2012, 2015). Negative correlation between CRS content and  $\chi_{lf}$  in sediment cores MD161/Stn8, MD161/Stn13, and NGHP-01-10D (Figure 9e) (Badesab et al., 2017) suggests that magnetic tracking in combination with geochemical proxies (CRS,  $\delta^{34}\text{S}_{\text{CRS}}$ , Mo) can be used to constrain paleo-SMTZ and methane seepage events in marine sediments.

#### 4.5 Conceptual magnetic mineralogical model to constrain gas hydrate evolution in K-G basin.

Based on the magnetic mineralogical signatures recorded in four sediment cores (NGHP-01-10D, NGHP-01-03B, NGHP-01-05C, and NGHP-01-07B) a conceptual model is proposed to constrain the influence of natural geological and sedimentary processes on the dynamics of the fracture-filled gas hydrate system of K-G basin (Figures 10a-10d). Tectonic changes, erosion process in the Himalayan mountain ranges, and intensification of the Asian summer monsoon delivered a huge terrigenous sediment load to K-G basin through activation of peninsular rivers that resulted in formation of a deep gas reservoir (Collins et al., 1999; Chauhan et al., 1993, 2004; Krishna et al., 2016; Sangode et al., 2001; Weber et al., 1997). Higher sedimentation rate events resulted in formation of local sediment depocentres (proximal) and shale bulges (distal) (Choudhari et al., 2010), which coincide with magneto-zone Z-III. Highly pressurized sediment strata that developed as a result of continued rapid sedimentation events triggered growth of a fault system that acted as a conduit for fluid/gas migration in Z-III. Fault growth facilitated trapping, burial, and preservation of

magnetite-rich sediment, which along with the mass transport deposits formed the magnetically enhanced Z-III. As sedimentation continued, sediment pore pressure increased significantly leading to short-term expulsion and migration of methane-rich fluids through a fault network that generated local H<sub>2</sub>S gradients produced as a result of AOM-coupled sulfate reduction in the vicinity of faults and fractures. When H<sub>2</sub>S was abundant, as will be the case when methane fluxes are high, pyritization reactions proceeded to completion so that pyrite dominated over intermediate sulfides such as greigite thereby creating distinct  $\chi_{\text{lf}}$  drops in Z-III. Larrasoana et al. (2007) showed this with extensive iron sulfide formation (mainly pyrite) occurring along faults and in their immediate vicinity. Pyrite aggregates formed along faults which resulted in diagenetic depletion of magnetic signals and potentially indicate paleo-SMTZ positions. Methane migration through the GHSZ led to nucleation of gas hydrates along the fault, which later acted as a seal for fault system closure and subsequent trapping of methane gas and hydrate in K-G basin. Simultaneous sedimentation provided an impermeable seal for gas hydrate preservation in K-G basin. Z-I represents the present-day sedimentary and geochemical environment of K-G basin. Detrital iron-bearing minerals supplied through Indian river systems reacted with H<sub>2</sub>S generated by bacterial activity via organic matter decomposition and AOM-coupled sulfate reduction in Z-I to cause primary magnetic mineral dissolution and  $\chi_{\text{lf}}$  decrease.

## 5. Conclusions

We present magnetic, geochemical, and sedimentological records from three sediment cores that overlie methane hydrate deposits in K-G basin, offshore of India, Bay of Bengal. A linkage is evident between higher sedimentation events, magnetite enrichment, shale tectonism, and gas hydrate system development in K-G basin. Relatively uniform and enhanced  $\chi_{\text{lf}}$  values in Z-III for all studied cores reflects a period of higher sedimentation that had a dominant control on gas hydrate formation (Figure S2). Coarse titanomagnetite grains survived diagenesis because of rapid sedimentation and opening of a fault system that preserved a magnetic record of sedimentary processes, magnetic mineral diagenesis and shale-tectonism in K-G basin (Figure S2). The distinct magnetic susceptibility drop in GHSZ (Z-III) and Z-IV helps to track paleo-SMTZ fronts and provide clues about rapid SMTZ shifts caused by short-term variability in methane fluxes and sedimentation rates.

Determination of precise timings of methane expulsion is difficult, but methane release might have started soon after fault system activation as evident by growth of pyrite aggregates induced by movement of H<sub>2</sub>S-rich fluids through the fault/fracture network. Investigations of additional

sediment cores from nearshore and shelf regions of K-G basin is required to identify precisely the sediment depocenters and to detect sites of active cold seepage associated with shale bulges or sediment ridges. Our work demonstrates the potential use of magnetic mineralogical signatures to explore for gas hydrates in a highly dynamic and complex marine gas hydrate-bearing sedimentary system. A conceptual model is presented to explain the control of shale-tectonism and rapid sedimentation on gas hydrate formation in the complex fracture-filled sedimentary system of K-G basin (Figures 10a-10d). The magnetic mineralogical approach presented here has wide scope and can be applied to other gas hydrate forming sedimentary environments.

### **Acknowledgements**

This study was funded by SERB-DST, Government of India, under the Early Career Research Award scheme (DST no: ECR/2016/000528) to FB. The National Gas Hydrate Program coordinated by DGH is thanked for providing sediment samples from Indian National Gas Hydrate Expedition 01 for this study. We thank the Directors of CSIR-NIO, NIOT, NCAOR, advisor MOES, and NGHP (India) for supporting this work. We thank T. Ramprasad, A. Mazumdar, and S. Iyer for suggestions, Daryl Vaz for technical support, and Girish Prabhu and Areef Sardar for assistance with XRD and SEM-EDS analysis at CSIR-NIO. We also thank the Director, Indian Institute of Geomagnetism (IIG), New Panvel, for allowing specialized rock magnetic measurements. We thank the Director of the Center for Advanced Marine Core Research (CMCR), Kochi University, Japan for access to the Paleomagnetic laboratory during a research visit of FB through an INSA-JSPS fellowship. These analyses were supported by DST-JSPS under the scheme JSPS Postdoctoral Fellowship for Overseas Researchers (Strategic Program) (JSPS grant GR 17202) and Establishment of Young Researcher Fellowship Programme 2017-2018 (No. IA/Indo-Japanese/F-1/2018) scheme awarded to FB. We thank Chisa Nishimori and Yuhji Yamamoto for providing support in Kochi. Additional data presented in this study are provided in the supporting information. The authors declare no conflicts of interests. This is CSIR-NIO publication no. xxx.

### **References**

Anitha, G., Ramana, M. V., Ramprasad, T., Dewangan, P., and Anuradha, M. (2014). Shallow geological environment of Krishna–Godavari offshore, eastern continental margin of India as inferred from the interpretation of high resolution sparker data. *Journal of Earth System Science*, 123(2), 329-342.

Archer, D., and Buffett B. (2005), Time-dependent response of the global ocean clathrate reservoir to climatic and anthropogenic forcing, *Geochemistry, Geophysics, Geosystems*, 6, Q03002, <https://doi:10.1029/2004GC000854>.

- Badesab, F., Dewangan, P., Usapkar, A., Kocherla, M., Peketi, A., Mohite, K., Sangode, S.J. and Deenadayalan, K. (2017). Controls on evolution of gas-hydrate system in the Krishna-Godavari basin, offshore India. *Geochemistry, Geophysics, Geosystems*, 18(1), pp.52-74. <https://doi.org/10.1002/2016GC006606>
- Bastia, R. (2007). Geologic Settings and Petroleum Systems of India's East Coast Offshore Basins: Concepts and Applications. *Technology Publications*.
- Berner, R. A. (1970). Sedimentary pyrite formation. *American Journal of Science*, 268(1), 1-23.
- Berner, R. A. (1984). Sedimentary pyrite formation: an update. *Geochimica et Cosmochimica Acta*, 48(4), 605-615. [https://doi.org/10.1016/0016-7037\(84\)90089-9](https://doi.org/10.1016/0016-7037(84)90089-9)
- Biksham, G., and Subramanian, V. (1988). Sediment transport of the Godavari River basin and its controlling factors. *Journal of Hydrology*, 101(1-4), 275-290. [https://doi.org/10.1016/0022-1694\(88\)90040-6](https://doi.org/10.1016/0022-1694(88)90040-6)
- Borowski, W. S., Paull, C. K., and Ussler III, W. (1996). Marine pore-water sulfate profiles indicate in situ methane flux from underlying gas hydrate. *Geology*, 24(7), 655-658. [https://doi.org/10.1130/0091-7613\(1996\)024<0655:MPWSPI>2.3.CO;2](https://doi.org/10.1130/0091-7613(1996)024<0655:MPWSPI>2.3.CO;2)
- Boswell, R., and Collett, T. S. (2011). Current perspectives on gas hydrate resources. *Energy and Environmental Science*, 4(4), 1206-1215.
- Canfield, D. E. (1989). Reactive iron in marine sediments. *Geochimica et Cosmochimica Acta*, 53(3), 619-632. [https://doi.org/10.1016/0016-7037\(89\)90005-7](https://doi.org/10.1016/0016-7037(89)90005-7)
- Canfield, D. E., and Berner, R. A. (1987). Dissolution and pyritization of magnetite in anoxic marine sediments. *Geochimica et Cosmochimica Acta*, 51(3), 645-659. [https://doi.org/10.1016/0016-7037\(87\)90076-7](https://doi.org/10.1016/0016-7037(87)90076-7)
- Canfield, D. E., Raiswell, R., and Bottrell, S. H. (1992). The reactivity of sedimentary iron minerals toward sulfide. *American Journal of Science*, 292(9), 659-683. <https://doi.org/10.2475/ajs.292.9.659>
- Chang, L., Roberts, A. P., Rowan, C. J., Tang, Y., Pruner, P., Chen, Q., and Horng, C. S. (2009). Low-temperature magnetic properties of greigite (Fe<sub>3</sub>S<sub>4</sub>). *Geochemistry, Geophysics, Geosystems*, 10(1). <https://doi.org/10.1029/2008GC002276>
- Chang, L., Bolton, C.T., Dekkers, M.J., Hayashida, A., Heslop, D., Krijgsman, W., Kodama, K., Paterson, G.A., Roberts, A.P., Rohling, E.J., and Yamamoto, Y. (2016). Asian monsoon modulation of nonsteady state diagenesis in hemipelagic marine sediments offshore of Japan. *Geochemistry, Geophysics, Geosystems*, 17(11), pp.4383-4398. <https://doi.org/10.1002/2016GC006344>
- Chang, L., Heslop, D., Roberts, A. P., Rey, D., and Mohamed, K. J. (2016a). Discrimination of biogenic and detrital magnetite through a double Verwey transition temperature. *Journal of Geophysical Research: Solid Earth*, 121(1), 3-14. <https://doi.org/10.1002/2015JB012485>
- Chang, L., Roberts, A.P., Heslop, D., Hayashida, A., Li, J., Zhao, X., Tian, W., and Huang, Q., (2016b). Widespread occurrence of silicate-hosted magnetic mineral inclusions in marine sediments and their contribution to paleomagnetic recording. *Journal of Geophysical Research: Solid Earth*, 121(12), pp.8415-8431. <https://doi.org/10.1002/2016JB013109>

- Chauhan, O. S., and Almeida, F. (1993). Influences of Holocene sea level, regional tectonics, and fluvial, gravity and slope currents induced sedimentation on the regional geomorphology of the continental slope off northwestern India. *Marine Geology*, 112(1-4), 313-328. [https://doi.org/10.1016/0025-3227\(93\)90176-V](https://doi.org/10.1016/0025-3227(93)90176-V)
- Chen, F., Hu, Y., Feng, D., Zhang, X., Cheng, S., Cao, J., and Chen, D. (2016). Evidence of intense methane seepages from molybdenum enrichments in gas hydrate-bearing sediments of the northern South China Sea. *Chemical Geology*, 443, 173-181. <https://doi.org/10.1016/j.chemgeo.2016.09.029>
- Choudhuri, M., Guha, D., Dutta, A., Sinha, S., and Sinha, N. (2006). Spatio-temporal variations and kinematics of shale mobility in the Krishna-Godavari basin, India. In: *AAPG Hedberg Conference, Port of Spain, Trinidad and Tobago, 5<sup>th</sup>-7<sup>th</sup> June, 2006*.
- Clift, P. D., Hodges, K. V., Heslop, D., Hannigan, R., Van Long, H., and Calves, G. (2008). Correlation of Himalayan exhumation rates and Asian monsoon intensity. *Nature Geoscience*, 1(12), 875. <http://dx.doi.org/10.1038/ngeo351>
- Colin, C., Turpin, L., Bertaux, J., Desprairies, A., and Kissel, C. (1999). Erosional history of the Himalayan and Burman ranges during the last two glacial–interglacial cycles. *Earth and Planetary Science Letters*, 171(4), 647-660. [https://doi.org/10.1016/S0012-821X\(99\)00184-3](https://doi.org/10.1016/S0012-821X(99)00184-3)
- Collett, T., Riedel, M., Cochran, J. R., Boswell, R., Presley, J., Kumar, P., Sathe, A., Lall, M., Sibal, V., and the NGHP Expedition 01 Scientists (2008). Indian National Gas Hydrate Program, *Expedition - 01, Initial report*, Directorate General of Hydrocarbons, Ministry of Petroleum and Natural gas, India.
- Collett, T.S., Boswell, R., Cochran, J.R., Kumar, P., Lall, M., Mazumdar, A., Ramana, M.V., Ramprasad, T., Riedel, M., Sain, K., and Sathe, A.V. (2014). Geologic implications of gas hydrates in the offshore of India: Results of the National Gas Hydrate Program Expedition 01. *Marine and Petroleum Geology*, 58, pp.3-28. <https://doi.org/10.1016/j.marpetgeo.2014.07.021>
- Cragg, B. A., Parkes, R. J., Fry, J. C., Weightman, A. J., Rochelle, P. A., and Maxwell, J. R. (1996). Bacterial populations and processes in sediments containing gas hydrates (ODP Leg 146: Cascadia Margin). *Earth and Planetary Science Letters*, 139(3-4), 497-507. [https://doi.org/10.1016/0012-821X\(95\)00246-9](https://doi.org/10.1016/0012-821X(95)00246-9)
- Crémière, A., Lepland, A., Chand, S., Sahy, D., Condon, D.J., Noble, S.R., Martma, T., Thorsnes, T., Sauer, S., and Brunstad, H. (2016). Timescales of methane seepage on the Norwegian margin following collapse of the Scandinavian Ice Sheet. *Nature Communications*, 7, p.11509. <http://dx.doi.org/10.1038/ncomms11509>
- Cui, M., Wang, Z., Nageswara Rao, K., Sangode, S.J., Saito, Y., Chen, T., Kulkarni, Y.R., Naga Kumar, K.C.V., and Demudu, G. (2017). A mid-to late-Holocene record of vegetation decline and erosion triggered by monsoon weakening and human adaptations in the south-east Indian Peninsula. *The Holocene*, 27(12), pp.1976-1987. <https://doi.org/10.1177/0959683617715694,2017>.
- Cullen, J. L. (1981). Microfossil evidence for changing salinity patterns in the Bay of Bengal over the last 20 000 years. *Palaeogeography, Palaeoclimatology, Palaeoecology*, 35, 315-356. [https://doi.org/10.1016/0031-0182\(81\)90101-2](https://doi.org/10.1016/0031-0182(81)90101-2)

- Curray J.R., Emmel F.J., Moore D.G., and Raitt R.W. (1982). Structure, Tectonics, and Geological History of the Northeastern Indian Ocean. In: Nairn A.E.M., Stehli F.G. (eds) *The Ocean Basins and Margins*. Springer, Boston, MA [https://doi.org/10.1007/978-1-4615-8038-6\\_9](https://doi.org/10.1007/978-1-4615-8038-6_9)
- Dekkers, M. J. (1989). Magnetic properties of natural pyrrhotite. II. High- and low-temperature behaviour of Jrs and TRM as function of grain size. *Physics of the Earth and Planetary Interiors*, 57, 266–283. [https://doi.org/10.1016/0031-9201\(89\)90116-7](https://doi.org/10.1016/0031-9201(89)90116-7)
- Dewangan, P., Ramprasad, T., Ramana, M. V., Mazumdar, A., Desa, M., and Badasab, F. (2008). Shale Tectonics in the Continental Slope and Rise Regions of Krishna-Godavari Basin, Bay of Bengal: Implication in Gas-Hydrate Exploration. *In AGU Fall Meeting Abstracts*.
- Dewangan, P., Ramprasad T., Ramana M. V., Mazumdar A., Desa M., and Badesab F. K. (2010), Seabed morphology and gas venting features in the continental slope region of Krishna-Godavari basin, Bay of Bengal: Implications in gas-hydrate exploration, *Marine and Petroleum Geology*, 27(7),1628–1641, <https://doi.org/10.1016/j.marpetgeo.2010.03.015>.
- Dewangan, P., Sriram G., Ramprasad T., Ramana M. V., and Jaiswal P. (2011). Fault system and thermal regime in the vicinity of site NGHP-01-10, Krishna–Godavari basin, Bay of Bengal, *Marine and Petroleum Geology*, 28, 1899–1914, <https://doi:10.1016/j.marpetgeo.2011.03.009>.
- Dewangan, P., Basavaiah N., Badesab F. K., Usapkar A., Mazumdar A., Joshi R., and Ramprasad T. (2013), Diagenesis of magnetic minerals in a gas hydrate/cold seep environment off the Krishna–Godavari basin, Bay of Bengal, *Marine Geology*, 340, 57–70, <https://doi.org/10.1016/j.margeo.2013.04.016>.
- Dickens, G. R., O'Neil, J. R., Rea, D. K., and Owen, R. M. (1995). Dissociation of oceanic methane hydrate as a cause of the carbon isotope excursion at the end of the Paleocene. *Paleoceanography and Paleoclimatology*, 10(6), 965-971. <https://doi.org/10.1029/95PA02087>
- Dunlop, D. J., Özdemir, Ö., and Schmidt, P. W. (1997). Paleomagnetism and paleothermometry of the Sydney Basin 2. Origin of anomalously high unblocking temperatures. *Journal of Geophysical Research: Solid Earth*, 102(B12), 27285-27295. <https://doi.org/10.1029/97JB02478>
- Ebert, Y., Shaar, R., Emmanuel, S., Nowaczyk, N., and Stein, M. (2018). Overwriting of sedimentary magnetism by bacterially mediated mineral alteration. *Geology*, 46(4), 291-294. <https://doi.org/10.1130/G39706.1>
- Enkin, R. J., Baker, J., Nourgaliev, D., Iassonov, P., and Hamilton, T. S. (2007). Magnetic hysteresis parameters and Day plot analysis to characterize diagenetic alteration in gas hydrate-bearing sediments. *Journal of Geophysical Research: Solid Earth*, 112(B6). <https://doi.org/10.1029/2006JB004638>
- Esteban, L., Enkin, R. J., and Hamilton, T. (2008). Gas hydrates and magnetism: comparative geological settings for diagenetic analysis. In *ICGH. Proceedings of the 6th International Conference on Gas Hydrates* (pp. 1-9).
- Ferdelman, T. G., Fossing, H., Neumann, K., and Schulz, H. D. (1999). Sulfate reduction in surface sediments of the southeast Atlantic continental margin between 15 38'S and 27 57'S (Angola and Namibia). *Limnology and Oceanography*, 44(3), 650-661. <https://doi.org/10.4319/lo.1999.44.3.0650>

- Froelich, P., Klinkhammer, G.P., Bender, M.L., Luedtke, N.A., Heath, G.R., Cullen, D., Dauphin, P., Hammond, D., Hartman, B., and Maynard, V. (1979). Early oxidation of organic matter in pelagic sediments of the eastern equatorial Atlantic: suboxic diagenesis. *Geochimica et Cosmochimica Acta*, 43(7), pp.1075-1090. [https://doi.org/10.1016/0016-7037\(79\)90095-4](https://doi.org/10.1016/0016-7037(79)90095-4)
- García-Tortosa, F. J., Alfaro, P., Gibert, L., and Scott, G. (2011). Seismically induced slump on an extremely gentle slope (< 1) of the Pleistocene Tecopa paleolake (California). *Geology*, 39(11), 1055-1058. <https://doi.org/10.1130/G32218.1>
- Garming, J. F. L., Bleil, U., and Riedinger, N. (2005). Alteration of magnetic mineralogy at the sulfate–methane transition: analysis of sediments from the Argentine continental slope. *Physics of the Earth and Planetary Interiors*, 151(3-4), 290-308. <https://doi.org/10.1016/j.pepi.2005.04.001>
- Goto, S., Matsubayashi, O., and Nagakubo, S. (2016). Simulation of gas hydrate dissociation caused by repeated tectonic uplift events. *Journal of Geophysical Research: Solid Earth*, 121(5), pp.3200-3219. <https://doi.org/10.1002/2015JB012711>
- Harrison, R. J., and Feinberg, J. M. (2008). FORCinel: An improved algorithm for calculating first order reversal curve distributions using locally weighted regression smoothing. *Geochemistry, Geophysics, Geosystems*, 9(5). <https://doi.org/10.1029/2008GC001987>
- Hatfield, R. G., and Maher B. A. (2008), Suspended sediment characterization and tracing using a magnetic fingerprinting technique: Bassenthwaite Lake, Cumbria, UK, *Holocene*, 18, 105–115 <https://doi.org/10.1177/0959683607085600>.
- Hatfield, R. G., and Maher B. A. (2009), Holocene sediment dynamics in an upland temperate lake catchment: Climatic and land-use impacts in the English Lake District, *Holocene*, 19, 427–438, <https://doi.org/10.1177/0959683608101392>.
- Herbozo, G., Hübscher, C., Kaul, N., Wagner, M., Pecher, I., and Kukowski, N. (2013). Influence of recent depositional and tectonic controls on marine gas hydrates in Trujillo Basin, Peru Margin. *Marine Geology*, 340, 30-48. <https://doi.org/10.1016/j.margeo.2013.04.010>
- Hirt, A. M., and Gehring, A. U. (1991). Thermal alteration of the magnetic mineralogy in ferruginous rocks. *Journal of Geophysical Research: Solid Earth*, 96(B6), 9947-9953. <https://doi.org/10.1029/91JB00573>
- Hirt, A. M., Lowrie, W., Clendenen, W. S., and Kligfield, R. (1993). Correlation of strain and the anisotropy of magnetic susceptibility in the Onaping Formation: evidence for a near-circular origin of the Sudbury basin. *Tectonophysics*, 225(4), 231-254. [https://doi.org/10.1016/0040-1951\(93\)90300-9](https://doi.org/10.1016/0040-1951(93)90300-9)
- Hong, W. L., Solomon, E. A., and Torres, M. E. (2014b). A kinetic-model approach to quantify the effect of mass transport deposits on pore water profiles in the Krishna–Godavari Basin, Bay of Bengal. *Marine and Petroleum Geology*, 58, 223-232. <https://doi.org/10.1016/j.marpetgeo.2014.06.014>.



- Hong, C. S., and Chen, K. H. (2006). Complicated magnetic mineral assemblages in marine sediments offshore southwestern Taiwan: Possible influences of methane flux on the early diagenetic process. *Terrestrial, Atmospheric and Oceanic Sciences*, 17, 1009–1026. [https://doi.org/10.3319/TAO.2006.17.4.1009\(GH\)](https://doi.org/10.3319/TAO.2006.17.4.1009(GH))
- Hong, C. S., and Roberts, A. P. (2006). Authigenic or detrital origin of pyrrhotite in sediments?: Resolving a paleomagnetic conundrum. *Earth and Planetary Science Letters*, 241(3-4), 750-762. <https://doi.org/10.1016/j.epsl.2005.11.008>
- Hong, C. S., and Roberts, A. P. (2018). The low-temperature Besnus magnetic transition: Signals due to monoclinic and hexagonal pyrrhotite. *Geochemistry, Geophysics, Geosystems*, 19, 3364–3375. <https://doi.org/10.1029/2017GC007394>
- Housen, B. A., and Moskowitz, B. M. (2006). Depth distribution of magnetofossils in near-surface sediments from the Blake/Bahama Outer Ridge, western North Atlantic Ocean, determined by low-temperature magnetism. *Journal of Geophysical Research: Biogeosciences*, 111(G1). <https://doi.org/10.1029/2005JG000068>
- Housen, B. A., and Musgrave, R. J. (1996). Rock-magnetic signature of gas hydrates in accretionary prism sediments. *Earth and Planetary Science Letters*, 139(3-4), 509-519. [https://doi.org/10.1016/0012-821X\(95\)00245-8](https://doi.org/10.1016/0012-821X(95)00245-8)
- Hu, Y., Chen, L., Feng, D., Liang, Q., Xia, Z., and Chen, D. (2017). Geochemical record of methane seepage in authigenic carbonates and surrounding host sediments: A case study from the South China Sea. *Journal of Asian Earth Sciences*, 138, 51-61. <https://doi.org/10.1016/j.jseas.2017.02.004>
- Hustoft, S., Büinz, S., Mienert, J., and Chand, S. (2009). Gas hydrate reservoir and active methane-venting province in sediments on < 20 Ma young oceanic crust in the Fram Strait, offshore NW-Svalbard. *Earth and Planetary Science Letters*, 284(1-2), 12-24. <https://doi.org/10.1016/j.epsl.2009.03.038>
- Jahren, A. H., Conrad, C. P., Arens, N. C., Mora, G., and Lithgow-Bertelloni, C. (2005). A plate tectonic mechanism for methane hydrate release along subduction zones. *Earth and Planetary Science Letters*, 236(3-4), 691-704. <https://doi.org/10.1016/j.epsl.2005.06.009>
- Johnson, J. E., and Phillips, S. C. (2014). Reconstructing Paleo-Smt Positions On The Cascadia Margin Using Magnetic Susceptibility. *Final Scientific Report, Univ. of New Hampshire, Durham, NH (United States)*.
- Johnson, J. E., Phillips, S. C., Torres, M. E., Piñero, E., Rose, K. K., & Giosan, L. (2014). Influence of total organic carbon deposition on the inventory of gas hydrate in the Indian continental margins. *Marine and Petroleum Geology*, 58, 406-424. <https://doi.org/10.1016/j.marpetgeo.2014.08.021>
- Jørgensen, B. B. (1982). Mineralization of organic matter in the sea bed—the role of sulphate reduction. *Nature*, 296(5858), 643-645. <https://doi.org/10.1038/296643a0>
- Jørgensen, B. B., Böttcher, M. E., Lüschen, H., Neretin, L. N., and Volkov, I. I. (2004). Anaerobic methane oxidation and a deep H<sub>2</sub>S sink generate isotopically heavy sulfides in Black Sea sediments. *Geochimica et Cosmochimica Acta*, 68(9), 2095-2118. <https://doi.org/10.1016/j.gca.2003.07.017>

- Kao, S. J., Horng, C. S., Roberts, A. P., and Liu, K. K. (2004). Carbon–sulfur–iron relationships in sedimentary rocks from southwestern Taiwan: influence of geochemical environment on greigite and pyrrhotite formation. *Chemical Geology*, 203(1-2), 153-168. <https://doi.org/10.1016/j.chemgeo.2003.09.007>
- Karlin, R., and Levi, S. (1983). Diagenesis of magnetic minerals in recent haemipelagic sediments. *Nature*, 303(5915), 327. <http://dx.doi.org/10.1038/303327a0>
- Kars, M. M., and Kodma K. (2015a), Authigenesis of magnetic minerals in gas hydrate bearing sediments in the Nankai Trough, Offshore Japan, *Geochemistry, Geophysics, Geosystems*, 16, 947–961, <https://doi.org/10.1002/2014GC005614>.
- Kars, M., and Kodama, K. (2015b). Rock magnetic characterization of ferrimagnetic iron sulfides in gas hydrate-bearing marine sediments at Site C0008, Nankai Trough, Pacific Ocean, off-coast Japan. *Earth, Planets and Space*, 67(1), 118. <https://doi.org/10.1186/s40623-015-0287-y>
- Karstens, J., Haflidason, H., Becker, L.W., Berndt, C., Rüpke, L., Planke, S., Liebetrau, V., Schmidt, M., and Mienert, J. (2018). Glacigenic sedimentation pulses triggered post-glacial gas hydrate dissociation. *Nature Communications*, 9(1), p.635. <https://doi.org/10.1038/s41467-018-03043-z>
- Kasten, S., Freudenthal T., Gingele F. X., and Schulz H. D. (1998), Simultaneous formation of iron-rich layers at different redox boundaries in sediments of the Amazon deep-sea fan, *Geochimica et Cosmochimica Acta*, 62, 2253–2264, [https://doi.org/10.1016/S0016-7037\(98\)00093-3](https://doi.org/10.1016/S0016-7037(98)00093-3).
- Kasten, S., Zabel, M., Heuer, V., and Hensen, C. (2003). Processes and signals of nonsteady-state diagenesis in deep-sea sediments and their pore waters. *The South Atlantic in the Late Quaternary* (pp. 431-459). Springer, Berlin, Heidelberg. <https://doi.org/10.1016/j.gca.2007.08.019>
- Kennett, J. P., Cannariato, K. G., Hendy, I. L., and Behl, R. J. (2000). Carbon isotopic evidence for methane hydrate instability during Quaternary interstadials. *Science*, 288(5463), 128-133. <https://doi.org/10.1126/science.288.5463.128>
- Knittel, K., and Boetius, A. (2009). Anaerobic oxidation of methane: progress with an unknown process. *Annual Review of Microbiology*, 63, 311-334. <https://doi.org/10.1038/296643a0>
- Krishna, K. S., Ismaiel, M., Srinivas, K., Gopala Rao, D., Mishra, J., and Saha, D. (2016). Sediment pathways and emergence of Himalayan source material in the Bay of Bengal. *Current Science* 110. <https://doi.org/10.18520/cs/v110/i3/363-372>
- Kumar, P., Collett, T.S., Boswell, R., Cochran, J.R., Lall, M., Mazumdar, A., Ramana, M.V., Ramprasad, T., Riedel, M., Sain, K., and Sathe, A.V. (2014). Geologic implications of gas hydrates in the offshore of India: Krishna-Godavari Basin, Mahanadi Basin, Andaman Sea, Kerala–Konkan Basin. *Marine and Petroleum Geology*, 58, pp.29-98. <https://doi.org/10.1016/j.marpetgeo.2014.07.031>
- Kvenvolden, K. A. (1988). Methane hydrate-a major reservoir of carbon in the shallow geosphere?. *Chemical Geology*, 71(1-3), 41-51. [https://doi.org/10.1016/0009-2541\(88\)90104-0](https://doi.org/10.1016/0009-2541(88)90104-0)
- Kvenvolden, K. A. (1993). Gas hydrates-geological perspective and global change. *Reviews of Geophysics*, 31(2), 173-187. <https://doi.org/10.1029/93RG00268>

- Larrasoña, J. C., Roberts, A. P., Musgrave, R. J., Gràcia, E., Piñero, E., Vega, M., and Martínez-Ruiz, F. (2007). Diagenetic formation of greigite and pyrrhotite in gas hydrate marine sedimentary systems. *Earth and Planetary Science Letters*, 261(3-4), 350-366. <https://doi.org/10.1016/j.epsl.2007.06.032>
- Lascu, I., Einsle, J. F., Ball, M. R., and Harrison, R. J. (2018). The vortex state in geologic materials: A micromagnetic perspective. *Journal of Geophysical Research: Solid Earth*, 123, 7285–7304. <https://doi.org/10.1029/2018JB015909>
- Leslie, B.W., Hammond, D. E., Berelson, W. M., and Lund S. P. (1990). Diagenesis in anoxic sediments from the California continental borderland and its influence on iron, sulfur, and magnetite behaviour, *Journal of Geophysical Research*, 95, 4453–4470, <https://doi.org/10.1029/JB095iB04p04453>.
- Li, N., Feng, D., Chen, L., Wang, H., and Chen, D. (2016). Using sediment geochemistry to infer temporal variation of methane flux at a cold seep in the South China Sea. *Marine and Petroleum Geology*, 77, 835-845. <https://doi.org/10.1016/j.marpetgeo.2016.07.026>
- Lin, Q., Wang, J., Taladay, K., Lu, H., Hu, G., Sun, F., and Lin, R. (2016). Coupled pyrite concentration and sulfur isotopic insight into the paleo sulfate–methane transition zone (SMTZ) in the northern South China Sea. *Journal of Asian Earth Sciences*, 115, 547-556. <https://doi.org/10.1016/j.jseaes.2015.11.001>
- Mazumdar, A., Joao, H. M., Peketi, A., Dewangan, P., Kocherla, M., Joshi, R. K., and Ramprasad, T. (2012). Geochemical and geological constraints on the composition of marine sediment pore fluid: Possible link to gas hydrate deposits. *Marine and Petroleum Geology*, 38(1), 35-52. <http://dx.doi.org/10.1016/j.marpetgeo.2012.07.004>
- Milkov, A. V., and Sassen, R. (2002). Economic geology of offshore gas hydrate accumulations and provinces. *Marine and Petroleum Geology*, 19(1), 1-11. [https://doi.org/10.1016/S0264-8172\(01\)00047-2](https://doi.org/10.1016/S0264-8172(01)00047-2)
- Moore, G. F., and Strasser, M. (2016). Large mass transport deposits in Kumano Basin, Nankai Trough, Japan. In *Submarine Mass Movements and their Consequences* (pp. 371-379). Springer, Cham. [https://doi.org/10.1007/978-3-319-20979-1\\_37](https://doi.org/10.1007/978-3-319-20979-1_37)
- Moore, G. F., Boston, B. B., Strasser, M., Underwood, M. B., and Ratliff, R. A. (2015). Evolution of tectono-sedimentary systems in the Kumano Basin, Nankai Trough forearc. *Marine and Petroleum Geology*, 67, 604-616. <https://doi.org/10.1016/j.marpetgeo.2015.05.032>
- Moskowitz, B. M., Frankel, R. B., and Bazylinski, D. A. (1993). Rock magnetic criteria for the detection of biogenic magnetite. *Earth and Planetary Science Letters*, 120(3-4), 283-300. [https://doi.org/10.1016/0012-821X\(93\)90245-5](https://doi.org/10.1016/0012-821X(93)90245-5)
- Musgrave, R. J., Bangs, N. L., Larrasoña, J. C., Gràcia, E., Hollamby, J. A., and Vega, M. E. (2006). Rise of the base of the gas hydrate zone since the last glacial recorded by rock magnetism. *Geology*, 34(2), 117-120. <https://doi.org/10.1130/G22008.1>

- Muxworthy, A. R., and Dunlop, D. J. (2002). First-order reversal curve (FORC) diagrams for pseudo-single-domain magnetites at high temperature. *Earth and Planetary Science Letters*, 203(1), 369-382. [https://doi.org/10.1016/S0012-821X\(02\)00880-4](https://doi.org/10.1016/S0012-821X(02)00880-4)
- Muxworthy, A. R., and McClelland, E. (2000). Review of the low-temperature magnetic properties of magnetite from a rock magnetic perspective. *Geophysical Journal International*, 140(1), 101-114. <https://doi.org/10.1046/j.1365-246x.2000.00999.x>
- Neretin, L. N., Böttcher, M. E., Jørgensen, B. B., Volkov, I. I., Lüschen, H., and Hilgenfeldt, K. (2004). Pyritization processes and greigite formation in the advancing sulfidization front in the upper Pleistocene sediments of the Black Sea 1. *Geochimica et Cosmochimica Acta*, 68(9), 2081-2093. [https://doi.org/10.1016/S0016-7037\(03\)00450-2](https://doi.org/10.1016/S0016-7037(03)00450-2)
- Novosel, I., Spence, G. D., and Hyndman, R. D. (2005). Reduced magnetization produced by increased methane flux at a gas hydrate vent. *Marine Geology*, 216(4), 265-274. <https://doi.org/10.1016/j.margeo.2005.02.027>
- Nowaczyk, N. R. (2011). Dissolution of titanomagnetite and sulphidization in sediments from Lake Kinneret, Israel. *Geophysical Journal International*, 187(1), 34-44. <https://doi.org/10.1111/j.1365-246X.2011.05120.x>
- Oldfield, F., Maher, B. A., Donoghue, J., and Pierce, J. (1985). Particle-size related, mineral magnetic source sediment linkages in the Rhode River catchment, Maryland, USA. *Journal of the Geological Society*, 142, 1035–1046, <https://doi.org/10.1144/gsjgs.142.6.1035>.
- O'Reilly, W., Hoffmann, V., Chouker, A. C., Soffel, H. C., and Menyeh, A. (2000). Magnetic properties of synthetic analogues of pyrrhotite ore in the grain size range 1-24  $\mu\text{m}$ . *Geophysical Journal International*, 142(3), 669-683. <https://doi.org/10.1046/j.1365-246x.2000.00169.x>
- Özdemir, Ö., Dunlop, D. J., and Moskowitz, B. M. (2002). Changes in remanence, coercivity and domain state at low temperature in magnetite. *Earth and Planetary Science Letters*, 194(3-4), 343-358. [https://doi.org/10.1016/S0012-821X\(01\)00562-3](https://doi.org/10.1016/S0012-821X(01)00562-3)
- Pan, Y. X., Zhu, R. X., Banerjee, S. K., Gill, J., and Williams Q. (2000), Rock magnetic properties related to thermal treatment of siderite: Behavior and interpretation, *Journal of Geophysical Research*, 105, 783–794. doi: 10.1029/1999JB900358
- Panieri, G., Graves, C. A., and James, R. H. (2016). Paleo-methane emissions recorded in foraminifera near the landward limit of the gas hydrate stability zone offshore western Svalbard. *Geochemistry, Geophysics, Geosystems*, 17(2), 521-537. <https://doi.org/10.1002/2015GC006153>
- Passier, H. D., De Lange, G. J., and Dekkers, M. J. (2001). Magnetic properties and geochemistry of the active oxidation front and the youngest sapropel in the eastern Mediterranean Sea. *Geophysical Journal International*, 145(3), 604-614. <https://doi.org/10.1046/j.0956-540x.2001.01394.x>
- Passier, H. F., and Dekkers, M. J. (2002). Iron oxide formation in the active oxidation front above sapropel S1 in the eastern Mediterranean Sea as derived from low-temperature magnetism. *Geophysical Journal International*, 150(1), 230-240. <https://doi.org/10.1046/j.1365-246X.2002.01704.x>

- Paull, C. K., Ussler, W., and Dillon, W. P. (1991). Is the extent of glaciation limited by marine gas-hydrates?. *Geophysical Research Letters*, 18(3), 432-434. <https://doi.org/10.1029/91GL00351>
- Peketi, A., Mazumdar, A., Joshi, R. K., Patil, D. J., Srinivas, P. L., and Dayal, A. M. (2012), Tracing the paleo sulfate–methane transition zones and H<sub>2</sub>S seepage events in marine sediments: An application of C-S-Mo systematic. *Geochemistry, Geophysics, Geosystems*, 13, Q10007, <https://doi.org/10.1029/2012GC004288>.
- Peketi, A., Mazumdar, A., Joao, H. M., Patil, D. J., Usapkar, A., and Dewangan, P. (2015). Coupled C–S–Fe geochemistry in a rapidly accumulating marine sedimentary system: diagenetic and depositional implications. *Geochemistry, Geophysics, Geosystems*, 16(9), 2865-2883. <https://doi.org/10.1002/2015GC005754>
- Philips, S. C. (2018), Diagenetic degradation of paleoenvironmental signals in magnetic susceptibility in the northern Bay of Bengal, *The IRM Quarterly*, Winter 2017-2018, Vol. 27 No.4
- Phillips, S. C., Johnson, J. E., Clyde, W. C., Setera, J. B., Maxbauer, D. P., Severmann, S., and Riedinger, N. (2017). Rock magnetic and geochemical evidence for authigenic magnetite formation via iron reduction in coal-bearing sediments offshore Shimokita Peninsula, Japan (IODP Site C0020). *Geochemistry, Geophysics, Geosystems*, 18(6), 2076-2098. <https://doi.org/10.1002/2017GC006943>
- Phillips, S. C., Johnson, J. E., Giosan, L., and Rose, K. (2014). Monsoon-influenced variation in productivity and lithogenic sediment flux since 110 ka in the offshore Mahanadi Basin, northern Bay of Bengal. *Marine and Petroleum Geology*, 58, 502-525. <https://doi.org/10.1016/j.marpetgeo.2014.05.007>
- Pike, C. R., Roberts, A. P., and Verosub, K. L. (1999). Characterizing interactions in fine magnetic particle systems using first order reversal curves. *Journal of Applied Physics*, 85(9), 6660-6667. <https://doi.org/10.1063/1.370176>
- Prabhakar, K. N., and Zutshi, P.L. (1993). Evolution of southern part of Indian East Coast basin. *Journal of Geological Society of India*, 41, 215-230.
- Prajith, A., Tyagi, A., and Kurian, P. J. (2018). Changing sediment sources in the Bay of Bengal: Evidence of summer monsoon intensification and ice-melt over Himalaya during the Late Quaternary. *Palaeogeography, Palaeoclimatology, Palaeoecology*, 511 : 309-318 <https://doi.org/10.1016/j.palaeo.2018.08.016>
- Pratson, L.F. and Laine, E.P., (1989). The relative importance of gravity-induced versus current-controlled sedimentation during the Quaternary along the Mideast U.S. outer continental margin revealed by 3.5 kHz echo character. *Marine Geology*, 89: 87-126. [https://doi.org/10.1016/0025-3227\(89\)90029-7](https://doi.org/10.1016/0025-3227(89)90029-7)
- Prell, W. L., Hutson, W. H., Williams, D. F., Bé, A. W., Geitzenauer, K., and Molfino, B. (1980). Surface circulation of the Indian Ocean during the last glacial maximum, approximately 18,000 yr BP. *Quaternary Research*, 14(3), 309-336. [https://doi.org/10.1016/0033-5894\(80\)90014-9](https://doi.org/10.1016/0033-5894(80)90014-9)

- Ramesh R., and V. Subramanian (1988), Temporal, spatial and size variation in the sediment transport in the Krishna River basin, India, *Journal of Hydrology*, 98, 53–65. [https://doi.org/10.1016/0022-1694\(88\)90205-3](https://doi.org/10.1016/0022-1694(88)90205-3)
- Ramprasad, T., Dewangan, P., Ramana, M. V., Mazumdar, A., Karisiddaiah, S. M., Ramya, E. R., and Sriram, G. (2011). Evidence of slumping/sliding in Krishna–Godavari offshore basin due to gas/fluid movements. *Marine and Petroleum Geology*, 28(10), 1806-1816. <https://doi.org/10.1016/j.marpetgeo.2011.02.007>
- Rao, G. N. (2001). Sedimentation, stratigraphy, and petroleum potential of Krishna-Godavari basin, East Coast of India. *American Association of Petroleum Geologists bulletin*, 85(9), 1623-1643.
- Rao, V. P. (1991). Clay mineral distribution in the continental shelf sediments from Krishna to Ganges river mouth, east coast of India.
- Rao, V. P., and Kessarkar, P. M. (2001). Geomorphology and geology of the Bay of Bengal and the Andaman Sea. *The Indian Ocean: A Perspective*, AA Balkema Publishers, 2, 817-868.
- Rao, V. P., Reddy, N. P., and Rao, C. M. (1988). Clay mineral distribution in the shelf sediments off the northern part of the east coast of India. *Continental Shelf Research*, 8(2), 145-151.
- Riedel, M., Collett, T. S., and Shankar, U. (2011). Documenting channel features associated with gas hydrates in the Krishna–Godavari Basin, offshore India. *Marine Geology*, 279(1-4), 1-11. <https://doi.org/10.1016/j.margeo.2010.10.008>
- Riedinger, N., and Brunner, B. (2014). Data report: concentration and sulfur isotope composition of iron monosulfide and pyrite from sediments collected during IODP Expedition 316. In Kinoshita, M., Tobin, H., Ashi, J., Kimura, G., Lallemand, S., Sreaton, E.J., Curewitz, D., Masago, H., Moe, K.T., and the Expedition 314/315/316 Scientists, *Proc. IODP, 314/315/316: Washington, DC (Integrated Ocean Drilling Program Management International, Inc.)*. doi:10.2204/iodp.proc.314315316.223.2014
- Riedinger, N., Pfeifer, K., Kasten, S., Garming, J. F. L., Vogt, C., and Hensen, C. (2005). Diagenetic alteration of magnetic signals by anaerobic oxidation of methane related to a change in sedimentation rate. *Geochimica et Cosmochimica Acta*, 69(16), 4117-4126. <https://doi.org/10.1016/j.gca.2005.02.004>
- Roberts, A. P. (2015). Magnetic mineral diagenesis. *Earth-Science Reviews*, 151, 1-47. <https://doi.org/10.1016/j.earscirev.2015.09.010>
- Roberts, A. P., and Turner, G. M. (1993). Diagenetic formation of ferrimagnetic iron sulphide minerals in rapidly deposited marine sediments, South Island, New Zealand. *Earth and Planetary Science Letters*, 115(1-4), 257-273. [https://doi.org/10.1016/0012-821X\(93\)90226-Y](https://doi.org/10.1016/0012-821X(93)90226-Y)
- Roberts, A. P., Florindo, F., Larrasoña, J. C., O'Regan, M. A., and Zhao, X. (2010). Complex polarity pattern at the former Plio–Pleistocene global stratotype section at Vrica (Italy): Remagnetization by magnetic iron sulphides. *Earth and Planetary Science Letters*, 292(1-2), 98-111. <https://doi.org/10.1016/j.epsl.2010.01.025>

- Roberts, A. P., L. Chang, C. J. Rowan, C. S. Horng, and F. Florindo (2011), Magnetic properties of sedimentary greigite ( $\text{Fe}_3\text{S}_4$ ): An update, *Reviews of Geophysics*, 49, RG1002, <https://doi.org/10.1029/2010RG000336>.
- Roberts, A. P., Pike, C. R., and Verosub, K. L. (2000). First-order reversal curve diagrams: A new tool for characterizing the magnetic properties of natural samples. *Journal of Geophysical Research: Solid Earth*, 105(B12), 28461-28475. <https://doi.org/10.1029/2000JB900326>
- Roberts, A.P., Almeida, T.P., Church, N.S., Harrison, R.J., Heslop, D., Li, Y., Li, J., Muxworthy, A.R., Williams, W. and Zhao, X. (2017). Resolving the origin of pseudo-single domain magnetic behavior. *Journal of Geophysical Research: Solid Earth*, 122(12), pp.9534-9558. <https://doi.org/10.1002/2017JB014860>
- Roberts, A.P., Zhao, X., Harrison, R.J., Heslop, D., Muxworthy, A.R., Rowan, C.J., Larrasoana, J.C., and Florindo, F., (2018). Signatures of reductive magnetic mineral diagenesis from unmixing of first order reversal curves. *Journal of Geophysical Research: Solid Earth*, 123, 4500–4522. <https://doi.org/10.1029/2018JB015706>
- Rochette, P., Fillion, G., Ballou, R., Brunet, F., Ouladdiaf, B., and Hood, L. (2003). High pressure magnetic transition in pyrrhotite and impact demagnetization on Mars. *Geophysical Research Letters*, 30(13), 1683. <https://doi.org/10.1029/2003GL017359>
- Rochette, P., Fillion, G., Mattéi, J.-L., and Dekkers, M. J. (1990). Magnetic transition at 30–34 K in Fe<sub>7</sub>S<sub>8</sub>: Insight into a widespread occurrence of pyrrhotite in rocks. *Earth and Planetary Science Letters*, 98, 319–328. [https://doi.org/10.1016/0012-821X\(90\)90034-U](https://doi.org/10.1016/0012-821X(90)90034-U)
- Rochette, P., Lorand, J. P., Fillion, G., and Sautter, V. (2001). Pyrrhotite and the remanent magnetization of SNC meteorites: A changing perspective on Martian magnetism. *Earth and Planetary Science Letters*, 190, 1–12. [https://doi.org/10.1016/S0012-821X\(01\)00373-9](https://doi.org/10.1016/S0012-821X(01)00373-9)
- Rowan, C. J., and Roberts, A. P. (2006). Magnetite dissolution, diachronous greigite formation, and secondary magnetizations from pyrite oxidation: Unravelling complex magnetizations in Neogene marine sediments from New Zealand. *Earth and Planetary Science Letters*, 241(1-2), 119-137. <https://doi.org/10.1016/j.epsl.2005.10.017>
- Rowan, C. J., Roberts, A. P., and Broadbent, T. (2009). Reductive diagenesis, magnetite dissolution, greigite growth and paleomagnetic smoothing in marine sediments: A new view. *Earth and Planetary Science Letters*, 277(1-2), 223-235. <https://doi.org/10.1016/j.epsl.2008.10.016>
- Sager, W. W., and Hall, S. A. (1991). Magnetic properties of black mud turbidites from ODP Leg 116, distal Bengal Fan. American Association of Petroleum Geologists, 75:3; Conference: *Annual meeting of the American Association of Petroleum Geologists (AAPG)*, Dallas, TX (United States), 7-10 Apr 1991
- Sangode, S. J., Sinha R., Phartiyal B., Chauhan O. S., Mazari R. K., Bagati T. N., Suresh N., Mishra S., Kumar R., and Bhattacharjee P. (2007), Environmental magnetic studies on some quaternary sediments of varied depositional settings in the Indian sub-continent, *Quaternary International.*, 159, 102–118, <https://doi.org/10.1016/j.quaint.2006.08.015>.

- Sangode, S. J., Suresh, N., and Bagati, T. N. (2001). Godavari source in the Bengal fan sediments: results from magnetic susceptibility dispersal pattern. *Current Science*, 660-664.
- Schneider, A., Panieri, G., Lepland, A., Consolaro, C., Crémière, A., Forwick, M., Johnson, J.E., Plaza-Faverola, A., Sauer, S., and Knies, J., (2018). Methane seepage at Vestnesa Ridge (NW Svalbard) since the Last Glacial Maximum. *Quaternary Science Reviews*, 193, pp.98-117. <https://doi.org/10.1016/j.quascirev.2018.06.006>
- Shankar, U., and M. Riedel (2010), Seismic and heat flow constraints from the gas hydrate system in the Krishna-Godavari basin, India, *Marine Geology*, 276(1-4), 1-13, <https://doi.org/10.1016/j.margeo.2010.06.006>.
- Shanmugam, G. (2006). Deep-water processes and facies models: Implications for sandstone petroleum reservoirs (Vol. 5). *Handbook of petroleum exploration and production*, Elsevier.
- Shanmugam, G., Bloch, R.B., Mitchell, S.M., Beamish, G.W., Hodgkinson, R.J., Damuth, J.E., Straume, T., Syvertsen, S.E., and Shields, K.E., (1995). Basin-floor fans in the North Sea: sequence stratigraphic models vs. sedimentary facies. *American Association of Petroleum Geologists bulletin*, 79(4), pp.477-511.
- Shanmugam, G., Lehtonen, L. R., Straume, T., Syvertsen, S. E., Hodgkinson, R. J., and Skibeli, M. (1994). Slump and debris-flow dominated upper slope facies in the Cretaceous of the Norwegian and northern North Seas (61-67 N): Implications for sand distribution. *American Association of Petroleum Geologists bulletin*, 78(6), 910-937.
- Shi, M., Wu, H., Roberts, A.P., Zhang, S., Zhao, X., Li, H., Su, X., Yang, T., Chang, L., Hu, P. and Zhao, X., (2017). Tectonic, climatic, and diagenetic control of magnetic properties of sediments from Kumano Basin, Nankai margin, southwestern Japan. *Marine Geology*, 391, pp.1-12. <https://doi.org/10.1016/j.margeo.2017.07.006>
- Tarduno, J. A., Sager, W. W., and Nogi, Y. (1995). 25. Early cretaceous magnetostratigraphy and paleolatitudes from the mid-pacific mountains: Preliminary results bearing on guyot formation and pacific plate translation1.
- Thompson, R., and F. Oldfield (1986), *Environmental Magnetism*, 227 pp., Allen and Unwin, London.
- Torres, M.E., Trehu, A.M., Cespedes, N., Kastner, M., Wortmann, U.G., Kim, J.H., Long, P., Malinverno, A., Pohlman, J.W., Riedel, M., and Collett, T. (2008), Methane hydrate formation in turbidite sediments of northern Cascadia, IODP Expedition 311, *Earth and Planetary Science Letters*, 271, 170-180, <https://doi.org/10.1016/j.epsl.2008.03.061>.
- Treude, T., Niggemann, J., Kallmeyer, J., Wintersteller, P., Schubert, C. J., Boetius, A., and Jørgensen, B. B. (2005). Anaerobic oxidation of methane and sulfate reduction along the Chilean continental margin. *Geochimica et Cosmochimica Acta*, 69(11), 2767-2779. <https://doi.org/10.1016/j.gca.2005.01.002>



- Usapkar, A., Dewangan, P., Kocherla, M., Ramprasad, T., Mazumdar, A., and Ramana, M. V. (2014). Enhanced methane flux event and sediment dispersal pattern in the Krishna–Godavari offshore basin: Evidences from rock magnetic techniques. *Marine and Petroleum Geology*, 58, 461-475. <https://doi.org/10.1016/j.marpetgeo.2014.08.008>
- van Dongen, B. E., Roberts, A. P., Schouten, S., Jiang, W.T., Florindo, F., and Pancost, R. D. (2007). Formation of iron sulfide nodules during anaerobic oxidation of methane. *Geochimica et Cosmochimica Acta*, 71, 5155–5167. <https://doi.org/10.1016/j.gca.2007.08.019>
- Verosub, K. L., and Roberts, A. P. (1995). Environmental magnetism: past, present, and future. *Journal of Geophysical Research: Solid Earth*, 100(B2), 2175-2192. <https://doi.org/10.1029/94JB02713>
- Verwey, E. J. W. (1939). Electronic conduction of magnetite (Fe<sub>3</sub>O<sub>4</sub>) and its transition point at low temperatures. *Nature*, 144(3642), 327. <http://dx.doi.org/10.1038/144327b0>
- von Huene, R., and Pecher, I. A. (1999). Vertical tectonics and the origins of BSRs along the Peru margin. *Earth and Planetary Science Letters*, 166(1-2), 47-55. [https://doi.org/10.1016/S0012-821X\(98\)00274-X](https://doi.org/10.1016/S0012-821X(98)00274-X)
- Wang, X., Hutchinson, D. R., Wu, S., Yang, S., and Guo, Y. (2011). Elevated gas hydrate saturation within silt and silty clay sediments in the Shenhu area, South China Sea. *Journal of Geophysical Research: Solid Earth*, 116(B5). <https://doi.org/10.1029/2010JB007944>
- Weber, M. E., Wiedicke, M. H., Kudrass, H. R., Hübscher, C., and Erlenkeuser, H. (1997). Active growth of the Bengal Fan during sea-level rise and highstand. *Geology*, 25(4), 315-318. [https://doi.org/10.1130/0091-7613\(1997\)025<0315:AGOTBF>2.3.CO;2](https://doi.org/10.1130/0091-7613(1997)025<0315:AGOTBF>2.3.CO;2)
- Wellsbury, P., Goodman, K., Cragg, B. A., and Parkes, R. J. (2000). The geomicrobiology of deep marine sediments from Blake Ridge containing methane hydrate (Sites 994, 995 and 997). In *Proceedings of the Ocean drilling program, Scientific results* (Vol. 164, pp. 379-391). College Station, TX: Ocean Drilling Program.
- Yamamoto, Y., Chiyonobu, S., Kanamatsu, T., Ahagon, N., Aoike, K., Kamiya, N., and Kinoshita, M. (2018). Repeated large-scale mass-transport deposits and consequent rapid sedimentation in the western part of the Bay of Bengal, India. *Geological Society, London, Special Publications*, 477, SP477-12. <https://doi.org/10.1144/SP477.12>
- Yu, X., Wang, J., Liang, J., Li, S., Zeng, X., and Li, W. (2014). Depositional characteristics and accumulation model of gas hydrates in northern South China Sea. *Marine and Petroleum Geology*, 56, 74-86. <https://doi.org/10.1016/j.marpetgeo.2014.03.011>

**Figure 1.** Location map of sediment cores NGHP-01-10D, NGHP-01-03B, NGHP-01-05C, NGHP-01-07B, MD161/Stn-8, and MD161/Stn-13 in the Krishna-Godavari (K-G) basin, Bay of Bengal.

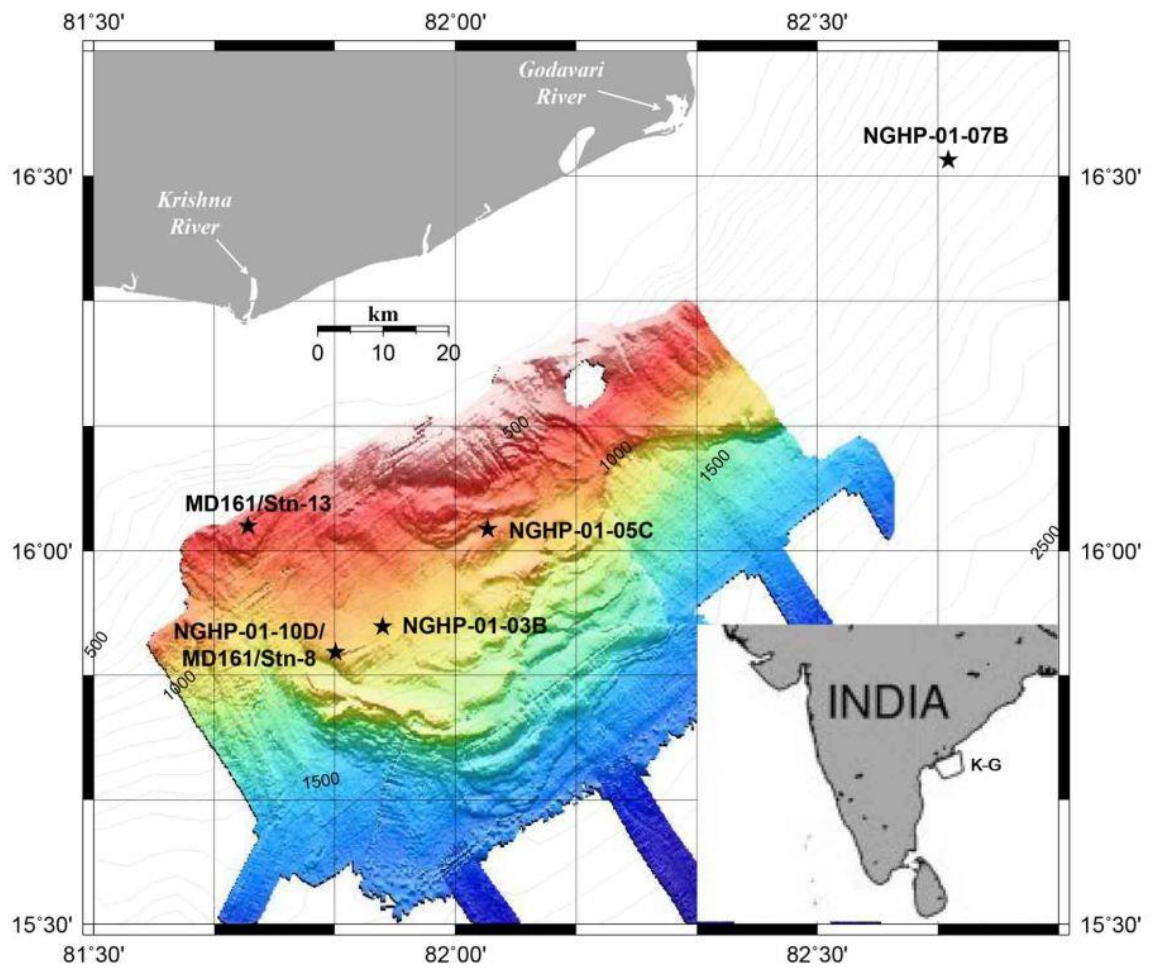


**Figure 2.** (a-d): Down-core variations of magnetic susceptibility ( $\chi$ ) in sediment cores (NGHP-01-10D, NGHP-01-03B, NGHP-01-05C, and NGHP-01-07B) from K-G basin. Increased magnetic susceptibility in zone -III is highlighted by a blue band. The distance between the core locations, depth of the bottom simulating reflector (BSR) and the position of the sulfate- methane transition zone (SMTZ) are also marked. Magnetic susceptibility data for core NGHP-01-10D are from Badesab et al. (2017).

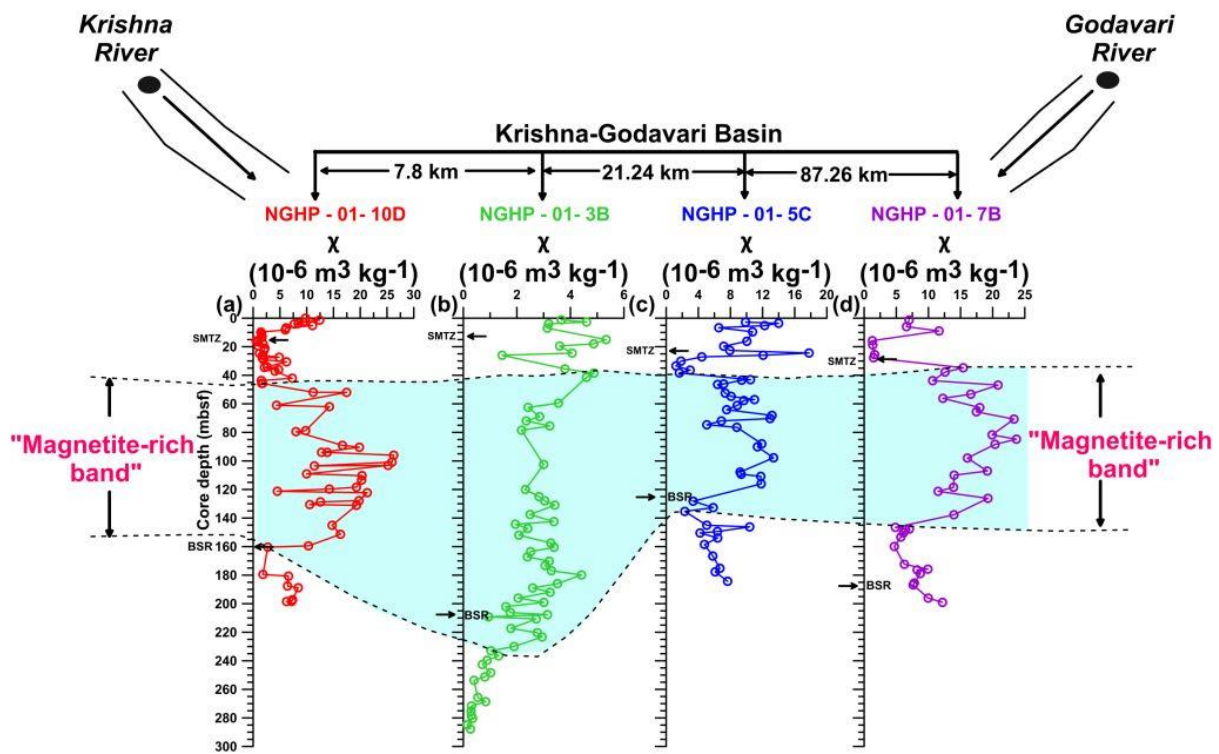


**Figure 3.** Depth variations of selected magnetic and sediment grain size data for sediment cores (a-e) NGHP-01-03B, (f-j) NGHP-01-05C, and (k-o) NGHP-01-07B. Data from discrete samples are color coded (zone-I: dark blue, zone-II: red, zone-III: green, zone-IV: purple) according to the sedimentary magneto-zones demarcated based on magnetic susceptibility variations. Increased magnetic susceptibility in zone-III is highlighted by a blue shading. The depths of the bottom simulating reflector (BSR), sulfate-methane transition zone (SMTZ), and the gas hydrate stability zone (GHSZ) are marked.

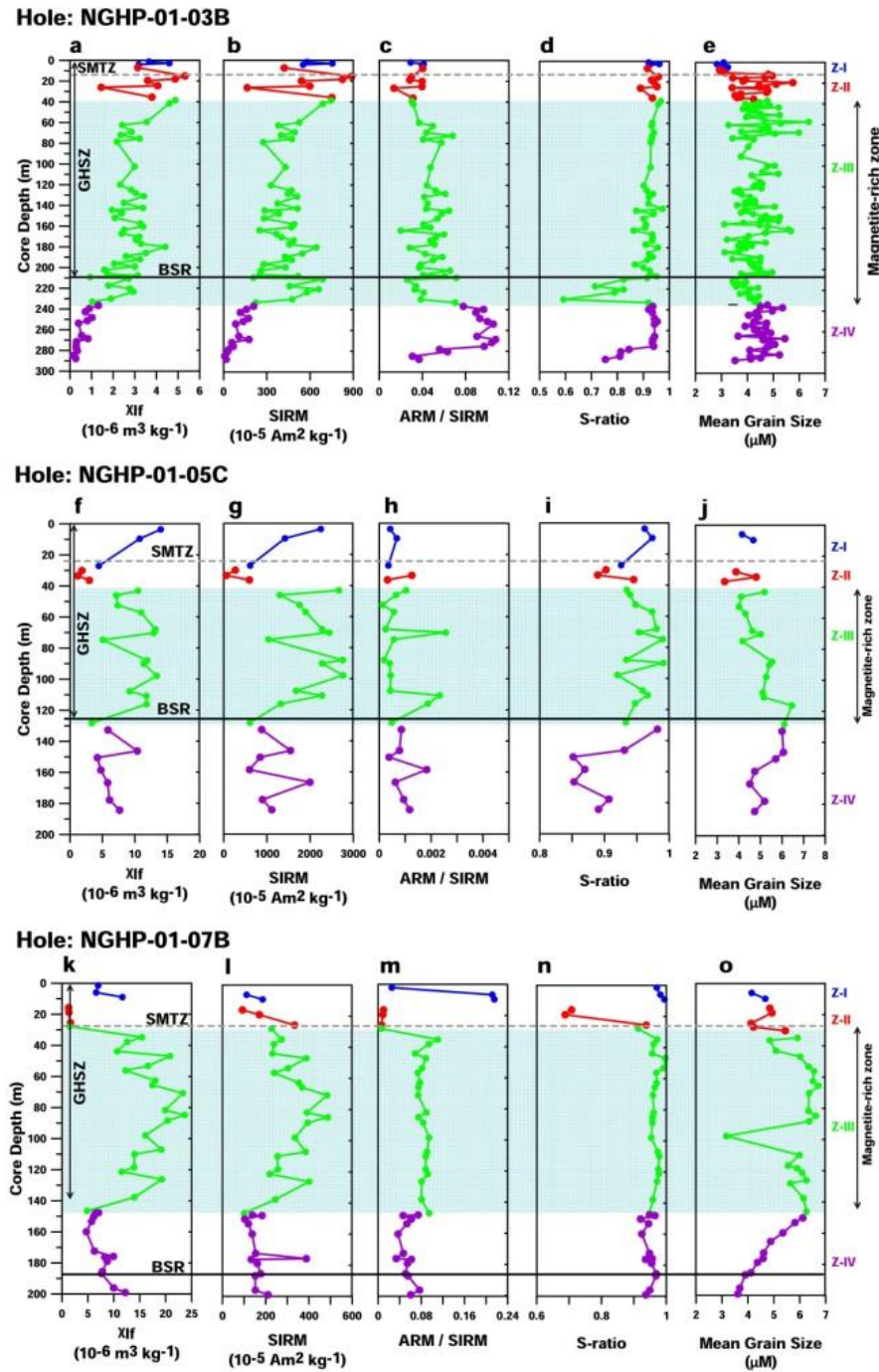


**Figure 4.** Temperature-dependence of magnetic susceptibility ( $\chi$ -T) for selected representative samples from the four sediment zones of the three studied sediment cores NGHP-01-03B, NGHP-01-05C, and NGHP-01-07B. Solid red lines indicate heating curves and blue lines indicate cooling curves.

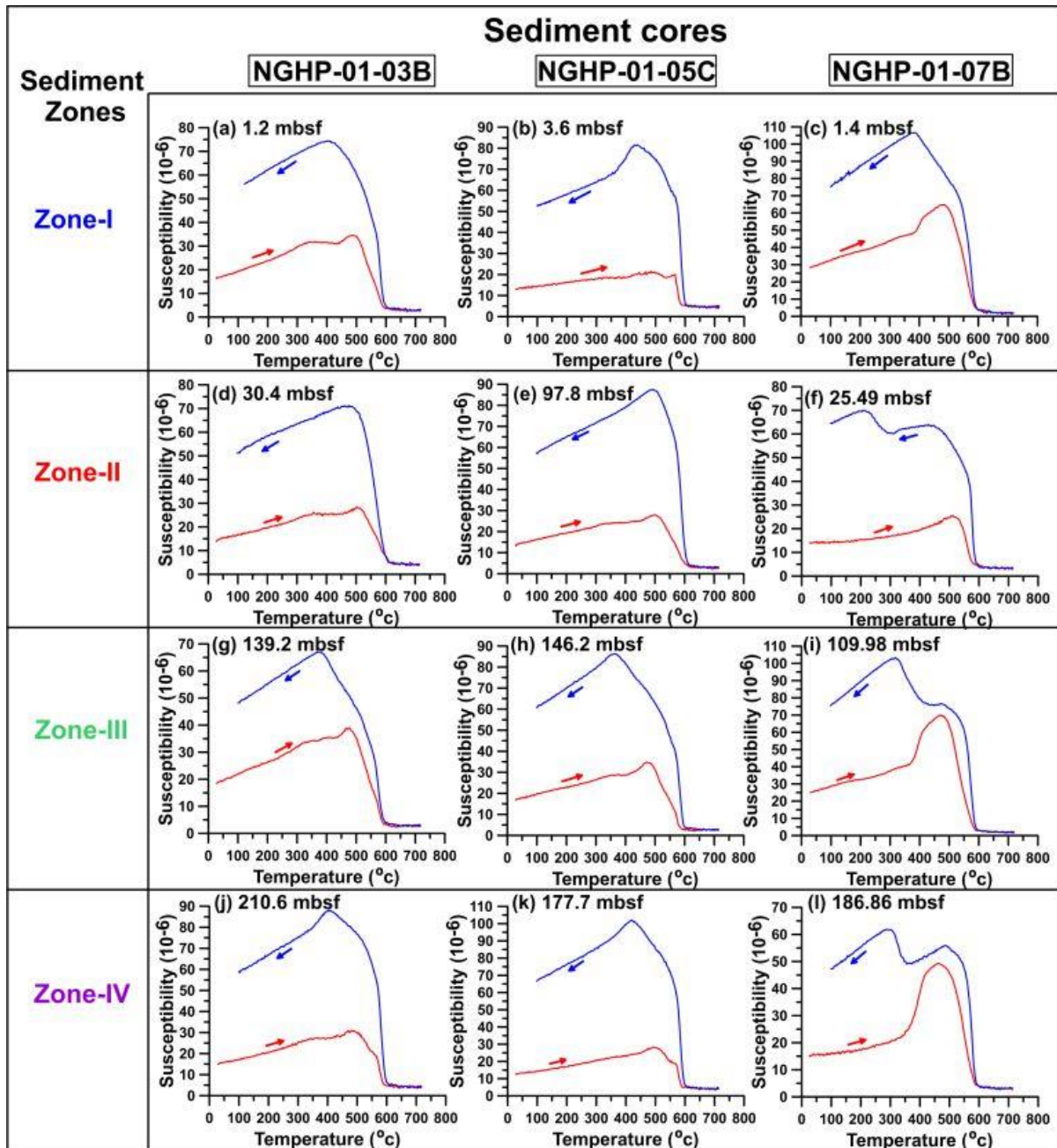


**Figure 5.** Low-temperature (< 300 K) magnetization curves for representative samples from the four sediment zones identified in sediment cores NGHP-01-05C and NGHP-01-07B. A distinct Verwey transition (for magnetite) and Besnus transition (for detrital pyrrhotite) is observed in the studied samples from different zones.

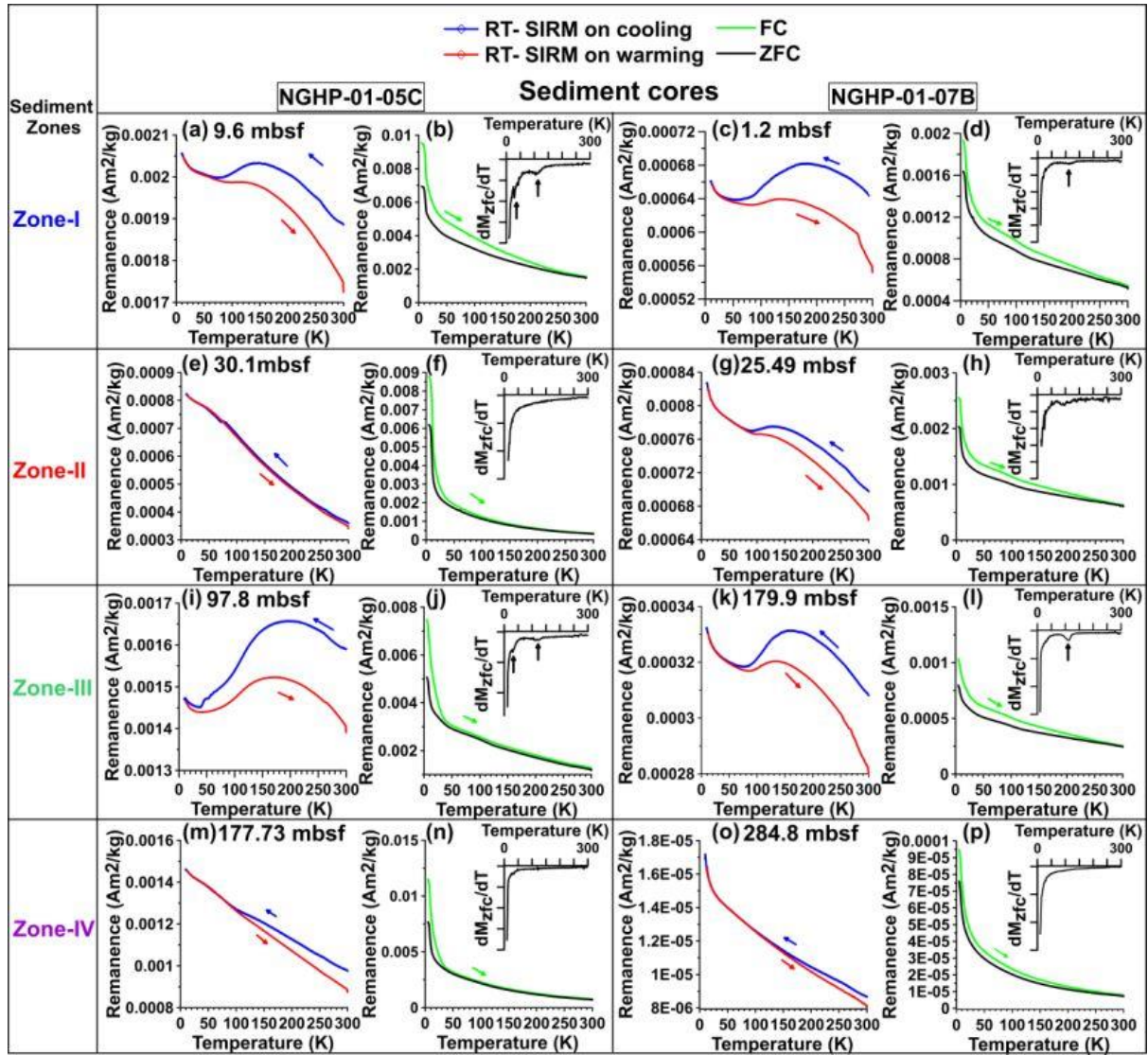


**Figure 6.** Representative FORC diagrams for the four sedimentary magneto-zones from cores NGHP-01-05C and NGHP-01-07B. All results are indicative of ferrimagnetic iron oxides, i.e., titanomagnetite in the vortex state (Roberts et al., 2017; Lascu et al., 2018).

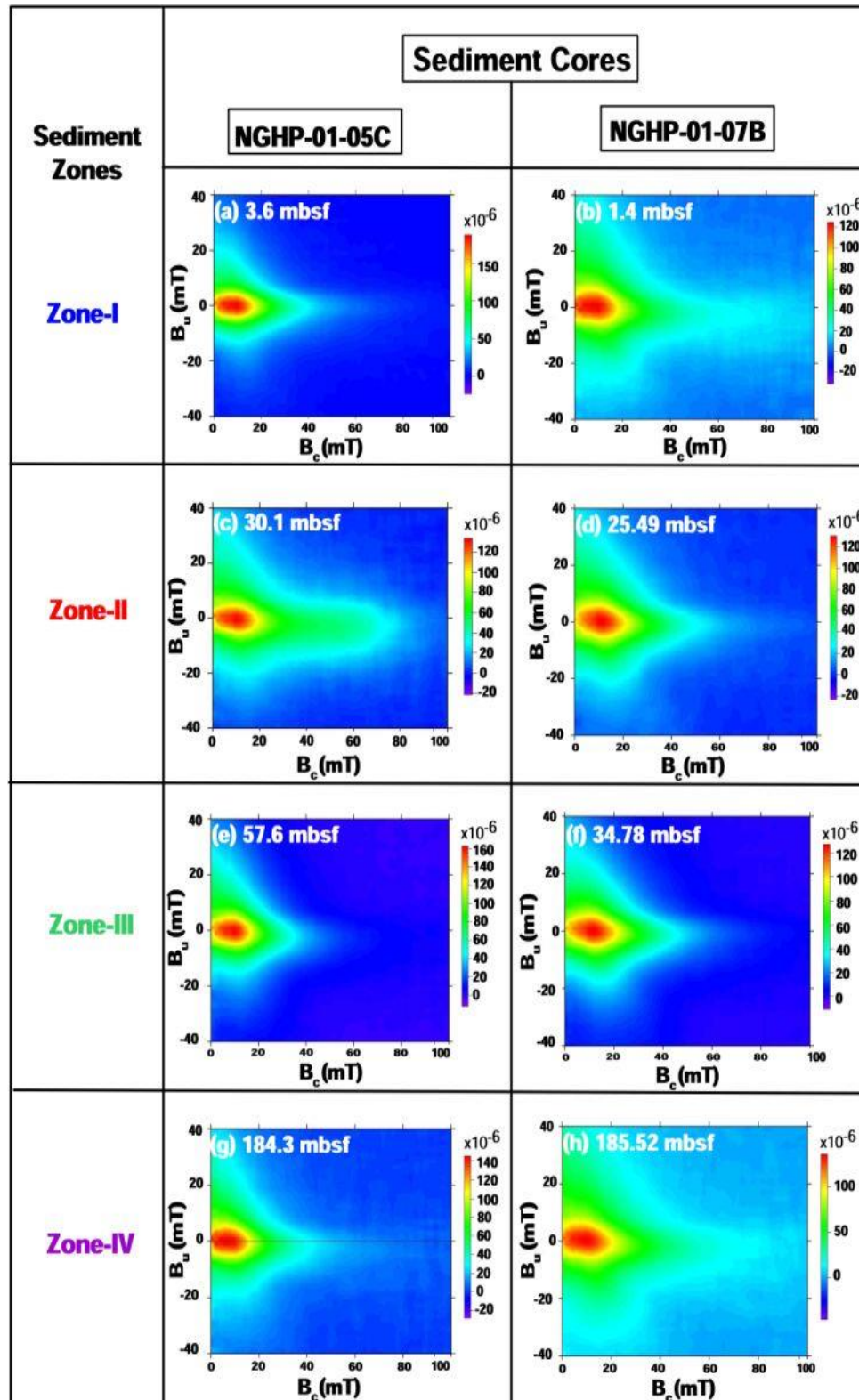


**Figure 7.** Scanning electron microscope images (secondary electron) on magnetic extracts from different sediment zones of NGHP-01-03B, NGHP-01-05C, and NGHP-01-07B. EDS spectra are placed adjacent to the respective images (a-l). Iron (Fe), titanium (Ti), sulfur (S), oxygen (O), calcium (Ca), silicon (Si), carbon (C), aluminum (Al), magnesium (Mg), potassium (K), zinc (Zn), and manganese (Mn) peaks are indicated.

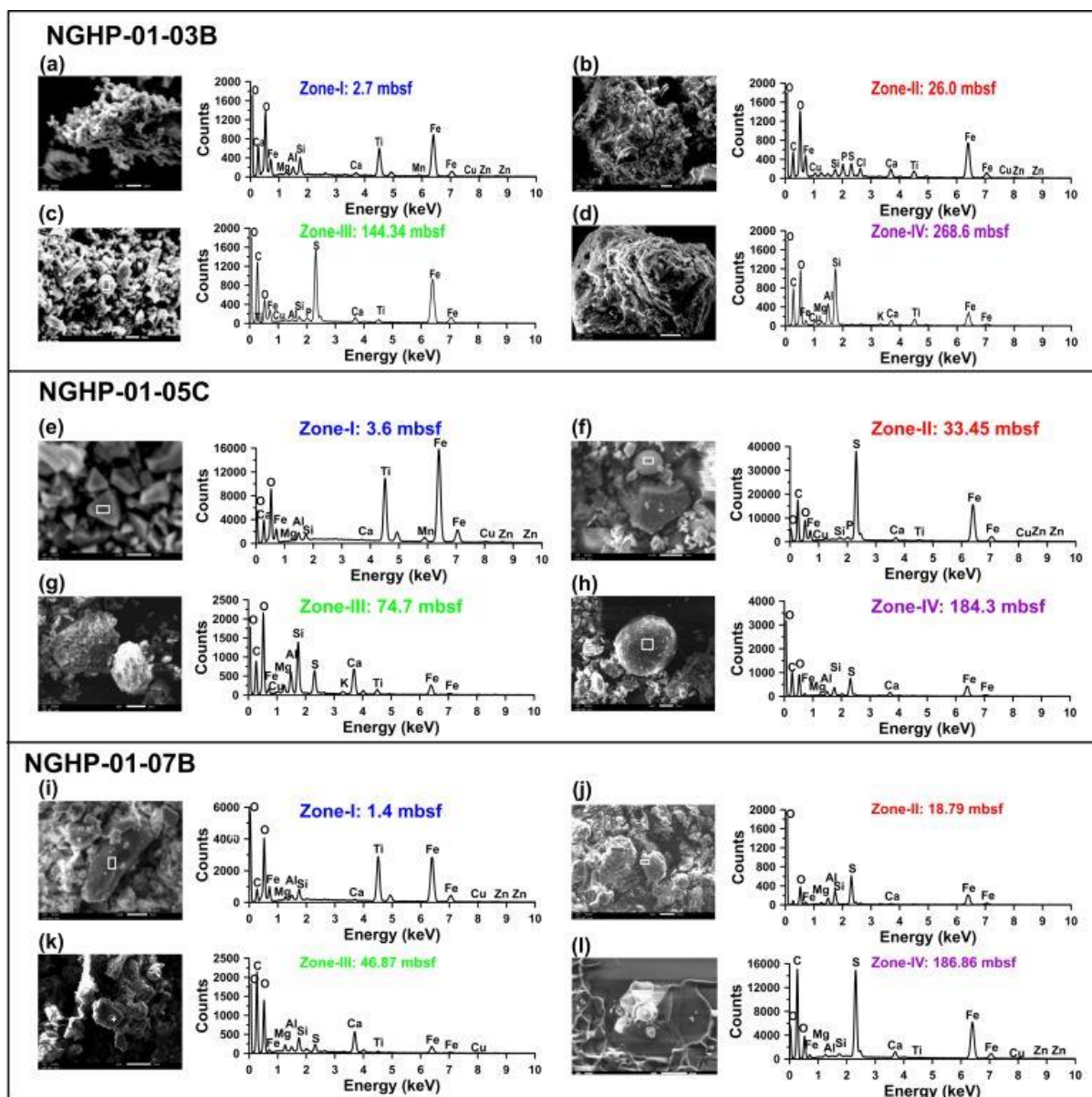




**Figure 8.** XRD spectra for minerals extracted from different sediment zones of cores (a-d) NGHP-01-03B, (e-h) NGHP-01-05C, and (i-l) NGHP-01-07B. TM: titanomagnetite, P: pyrite, Q: quartz.

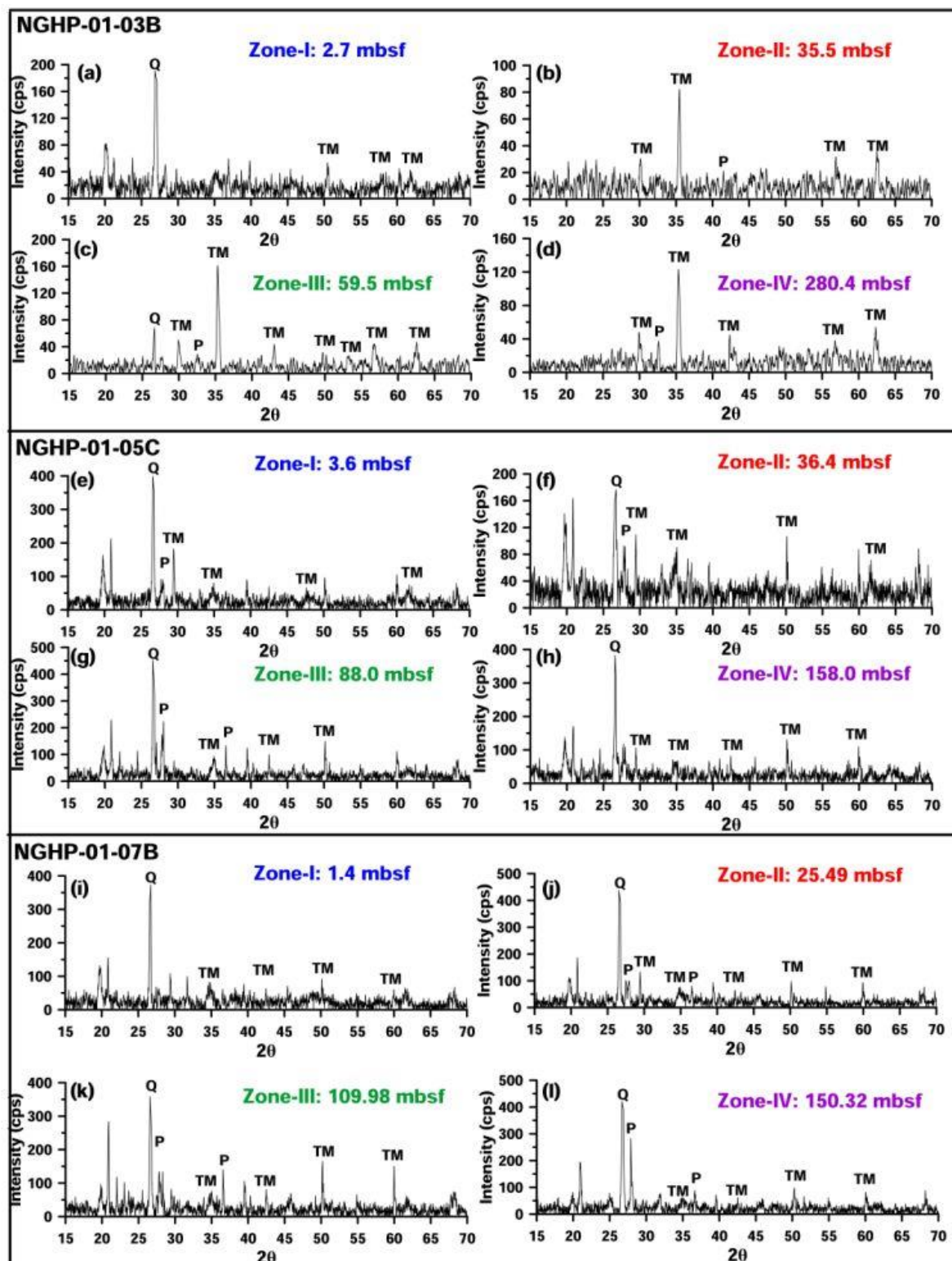


**Figure 9.** (a-c): Scatter plots of magnetic parameters ( $\chi$ , SIRM,  $\chi_{fd}\%$ , SIRM/ $\chi$ , and ARM/SIRM) for cores NGHP-01-10D, NGHP-01-03B, NGHP-01-05C, and NGHP-01-07B. (d)  $\delta_{FC}$  versus  $\delta Z_{FC}$  derived from low-temperature measurements (Moskowitz et al., 1993) for cores NGHP-01-05C and NGHP-01-07B. (e) Plot of CRS versus  $\chi_{if}$  for sediment cores NGHP-01-10D, MD161/Stn-8, and MD161/Stn-13. Note that gray arrows in the scatter plots are used to highlight trends. Magnetic and CRS data for sediment cores NGHP-01-10D, MD161/Stn-8, and MD161/Stn-13 are from Badesab et al. (2017) and Peketi et al. (2012, 2015).

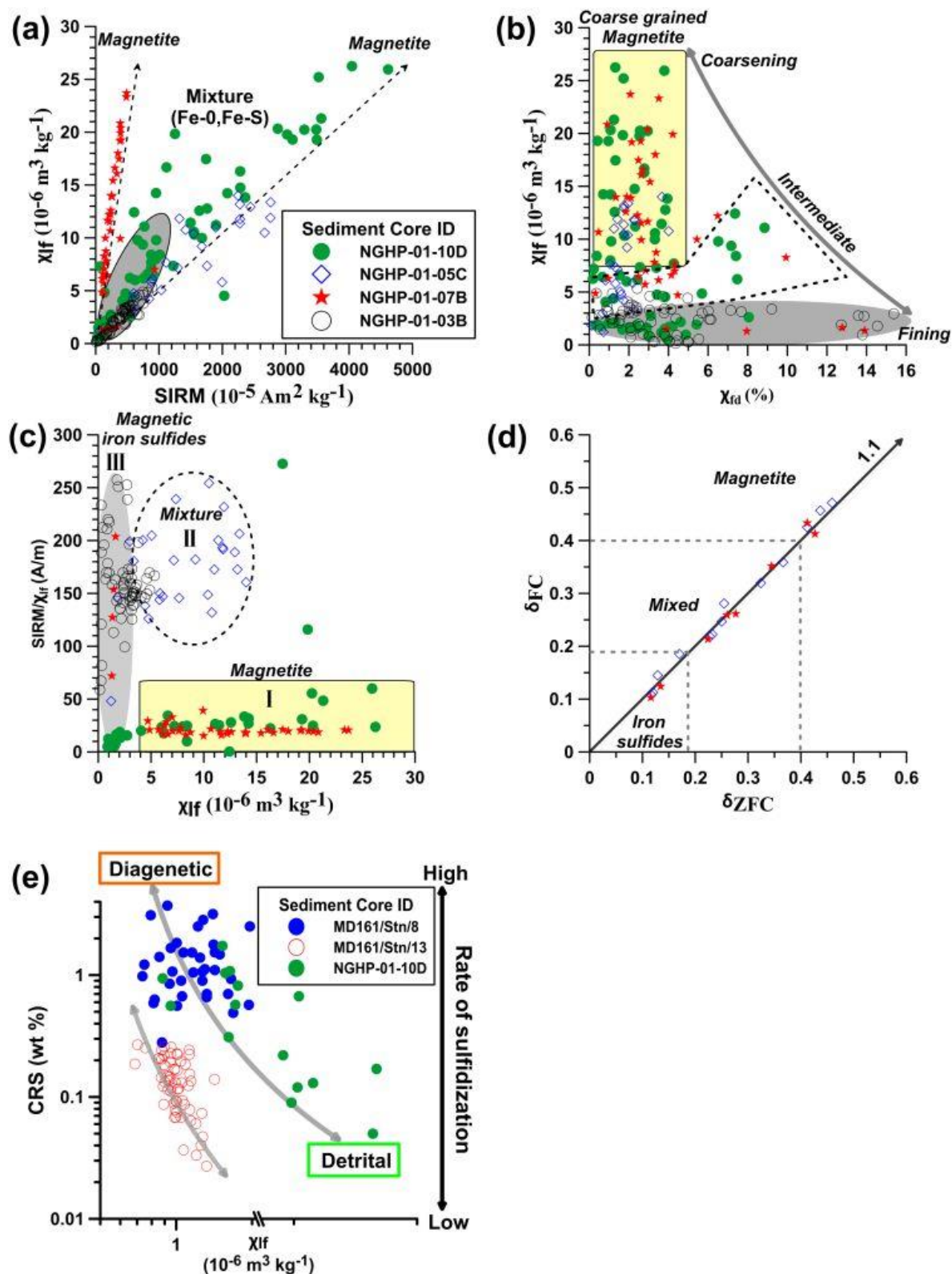
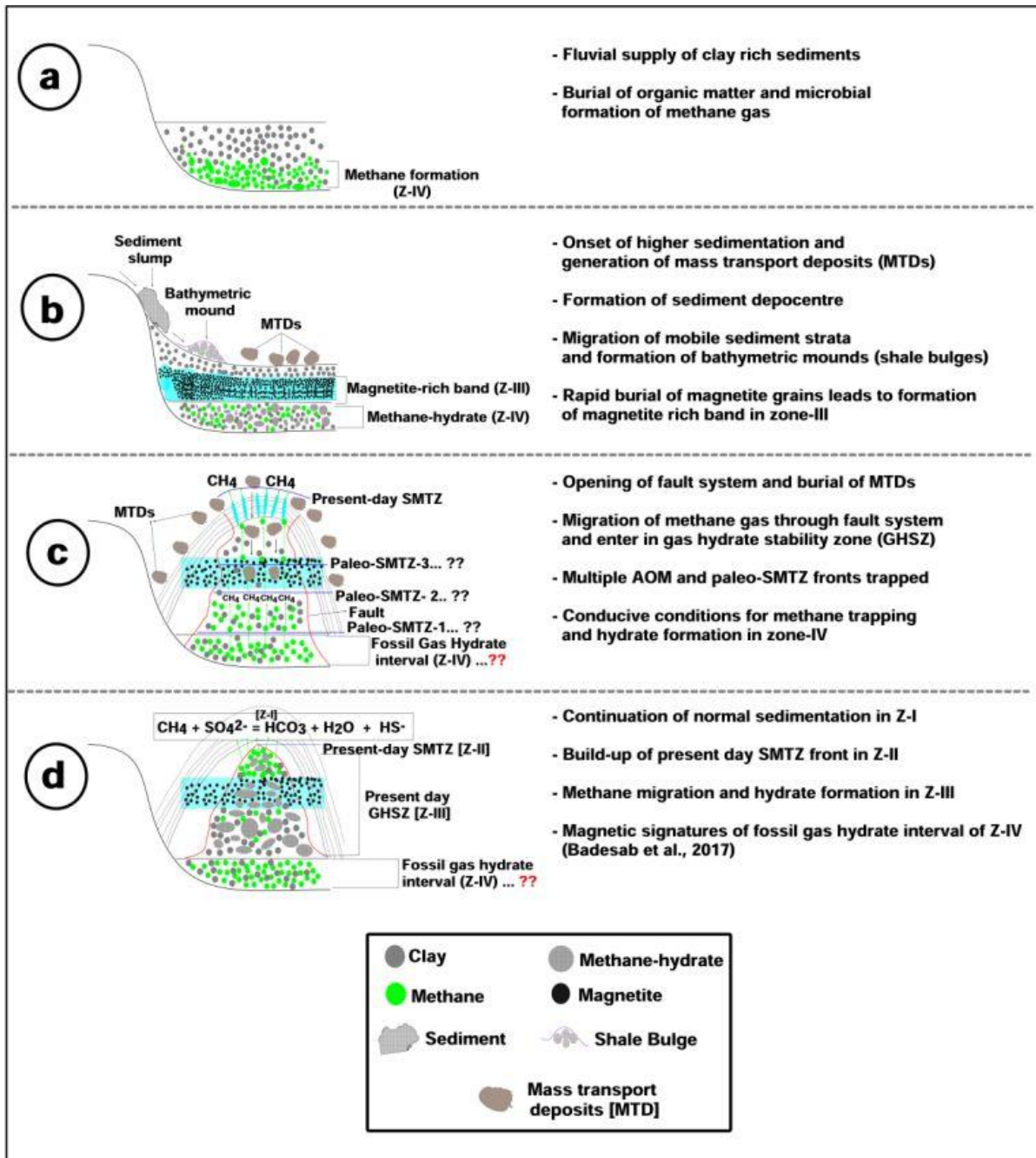


**Figure 10.** (a-d): Conceptual model for different controls (tectonic, sediment deposition, methane seepage dynamics, gas hydrates (formation/dissociation), and sediment diagenesis) on magnetic mineralogical variations observed in sediment cores NGHP-01-03B, NGHP-01-05C, and NGHP-01-07B.



**Supplementary Figures:**

**Figure S1.** Scanning electron microscope images of Fe-Ti and Fe-S particles in magnetically enhanced zone Z-III of sediment cores (a) NGHP-01-03B (Skeletal type titanohematite with lamellae), (b) NGHP-01-05C (pyrite overgrowth on titanomagnetite grain) and (c) NGHP-01-07B (well-preserved titanomagnetite grain).

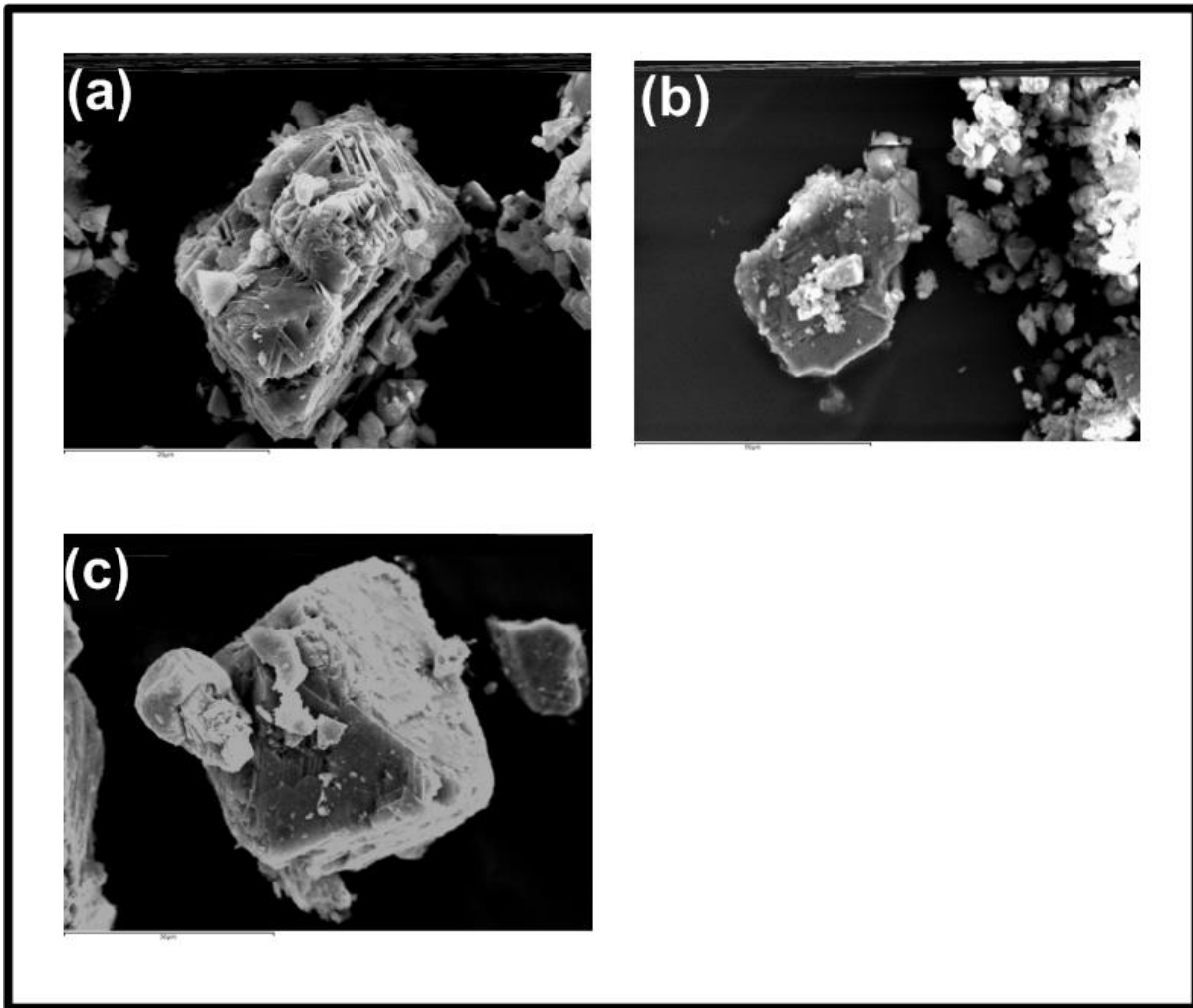


**Figure S2.** High resolution seismic (HRS) record of site NGHP-01-10D, NGHP-01-03B, and NGHP-01-05C showing various subsurface features such as finely layered sediments (FLS) which correspond to nannofossil-rich clay. The acoustically transparent layers as observed in the seismic section represents the MTDs (Ramprasad et al., 2011; Anitha et al., 2014). The magnetic susceptibility profiles of three cores are overlaid on the corresponding seismic section for better interpretations.

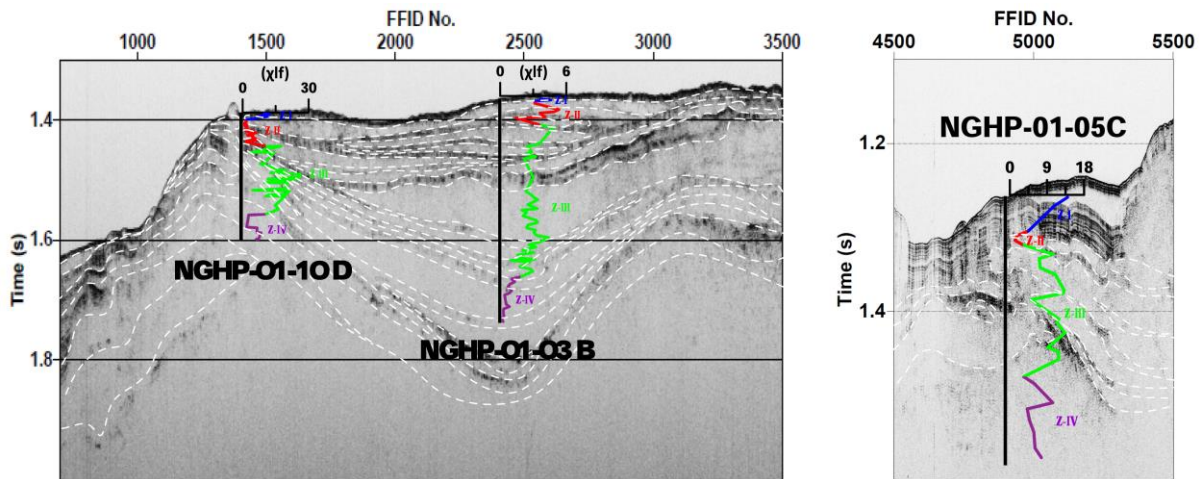


**Figure S3.** Pore-water data of sulfate (blue circles) and methane (red circles) of sediment cores (a) NGHP-01-10D (b) NGHP-01-03B (c) NGHP-01-05C and (d) NGHP-01-07B.

